were cryoprotected by 30% sucrose, and the coronal slices of 30-μm thickness were cut by a cryostat. The free floating serial coronal sections, from the rostral to the caudal edge of SNc or a part of the striatum, were incubated with rabbit anti-TH antibody (1:10,000; Millipore) or rabbit anti-AADC serum (1:20,000) (12), followed by biotinylated goat anti-rabbit IgG antibody (1:250; Vector Laboratories) and avidin-peroxidase complex (Vectastain ABC kit, Vector Laboratories). Immunocomplexes were visualized by a reaction with 3,3′-diaminobenzidine tetrahydrochloride and 0.003% H_2O_2. Images were taken using an upright microscope (Eclipse E800, Nikon) equipped with a cooled CCD camera (VB-6010, Keyence).

The numbers of TH-positive neurons in the injected and uninjected side SNc were compared using a stereological cell counting method. SNc was defined according to the brain atlas (22). Briefly, one in every three coronal sections covering the whole SNc was selected (typically 12–14 sections) and stained for TH, and magnified images of SNc were taken using a 20× objective lens (numerical aperture 0.5). For each region of interest, images were taken at multiple different focus planes to visualize all cells in the thickness. The number of all TH-positive cells in SNc in each slice was counted manually with ImageJ (National Institutes of Health). Only cells with an apparently visible nucleus were included. The number of all TH-positive neurons from a set of slices was summed (typically 1600–2000 cells in the uninjected side), and the ratio of the number in the injected side to that in the uninjected side was evaluated.

For fluorescence immunohistochemistry, the following secondary antibodies were used: Alexa546-conjugated anti-mouse IgG (1:2,000; Invitrogen) and Alexa633-conjugated anti-rabbit IgG (1:2,000; Invitrogen). Images were taken using the TCS SPE confocal microscope (Leica) with a 63× oil objective lens and excitation lasers of 532 and 635 nm.

For the detection of dopamine, we fixed mice transcardially with 5% glutaraldehyde, and the brain sections made with vibratome were stained with rabbit anti-TH antibody or rabbit anti-dopamine-glutaraldehyde conjugate (1:500; Millipore). Because glutaraldehyde fixation induces very strong background fluorescence, we performed immunodetection with the avidin-peroxidase complex as described above instead of fluorescence detection.

Western Blotting—To dissect striatal tissues for biochemical assays, we first made a coronal section of 2-mm thickness from approximately +1.5 to 0.5 mm to the bregma using a brain matrix (Neuroscience, Inc., Tokyo). Then the left and right dorsal striata were dissected by a surgical blade under a stereo microscope and homogenized using the Pellet Mixer (TreffLab) in 150 μl of PBS containing 1 mM dithiothreitol, 2 mM EDTA, 2 mM NaF, 1 μg/ml leupeptin, 1 μg/ml pepstatin, 1 mM phenylmethylsulfonyl fluoride, and 0.1 mM pargyline, followed by centrifugation at 20,000 × *g* for 10 min at 4 °C. An aliquot of the supernatant was used for the monoamine assay. In some experiments, ventral midbrain homogenates were prepared similarly, except the positions of coronal sections were approximately −2.5 to −4.5 mm to the bregma. The striatal or ventral midbrain homogenates containing 10 μg of protein were separated by electrophoresis on a 10% SDS-polyacrylamide gel and transferred to a PVDF membrane. The membranes were immunodetected using the following primary antibodies: rabbit anti-TH antibody (1:10,000; Millipore), rabbit anti-AADC antibody (1:20,000) (12), or mouse anti-β-actin antibody (1:10,000; Sigma-Aldrich). Immunoreactive proteins were detected by peroxidase-conjugated secondary antibodies and Immobilon-Western (Millipore). Quantitative analyses were performed with LAS-3000 (Fujifilm).

For better quantification of low level TH proteins by Western blot, we assessed the linearity of the detection using serial dilution of striatal homogenates of the uninjected side (supplemental Fig. 1). Then we employed a range showing a linear relationship between actual loaded proteins (2.5–20 μg, or a 0.125–1.0 ratio) and measured TH protein levels (0.05–1 ratio). Within this range, we made a standard curve and calibrated the TH protein levels accordingly.

For detection of vesicular monoamine transporter 2 (vMAT2) and dopamine transporter (DAT) proteins, a crude synaptosomal fraction was prepared by homogenizing striatal tissues in 4 mM HEPES buffer containing 0.32 M sucrose, 2 mM NaF, 1 μg/ml leupeptin, 1 μg/ml pepstatin, 1 mM phenylmethylsulfonyl fluoride, and 0.1 mM pargyline. The homogenate was centrifuged at 900 × *g*, the supernatant was further centrifuged at 14,500 × *g*, and the resulting pellet (P2 fraction) was dissolved in 80 μl of the same HEPES buffer containing 1% SDS. Protein concentration was determined by the DC protein assay (Bio-Rad). 20 μg of each protein sample was analyzed by Western blot using the following primary antibodies: rabbit anti-vMAT2 antiserum (1:500; Synaptic Systems), rabbit anti-DAT antibody (1:500; Millipore), rabbit anti-TH antibody (1:10,000; Millipore), or mouse anti-β-actin antibody (1:10,000; Sigma-Aldrich).

For the detection of phospho-TH proteins, striatal homogenates were prepared by immediate boiling of a whole brain for 5 min after dissection, followed by isolation of striata and homogenization and sonication in 0.1 M Tris-HCl (pH 6.8) buffer containing 1% SDS. Protein concentration was determined by the DC protein assay (Bio-Rad). 60 μg of each protein sample was analyzed by Western blot using the following primary antibodies: rabbit anti-Ser(P)-40-TH antibody (1:2,000; Millipore), rabbit anti-p31-TH antibody (1:2,000; Millipore), or rabbit anti-TH antibody (1:10,000; Millipore).

Monoamine Assay—Aliquots of striatal supernatant were deproteinized by 60 mM perchloric acid with 30 μM EDTA and 30 μM pargyline on ice for 30 min and centrifuged at 20,000 × *g* for 15 min. The monoamine levels in the supernatant were analyzed by high performance liquid chromatography (HPLC) with an SC5-ODS column (EICOM) and a mobile phase buffer containing 84 mM acetic acid-citrate (pH 3.5), 5 μg/ml EDTA, 190 mg/ml sodium 1-octane sulfonate, and 16% methanol. Monoamines were detected by electrochemical detection (ECD-100, EICOM).

Biopterin contents were measured as described previously (43). Briefly, the deproteinized homogenates were oxidized by 0.1 M HCl containing 0.1% I_2 and 0.2% KI for 1 h at room temperature, followed by centrifugation at 20,000 × *g* for 10 min. The supernatants were neutralized by 0.2% ascorbic acid and then subjected to HPLC analyses with Inertsil ODS-3 column (GL Sciences) and a mobile phase buffer containing 10 mM

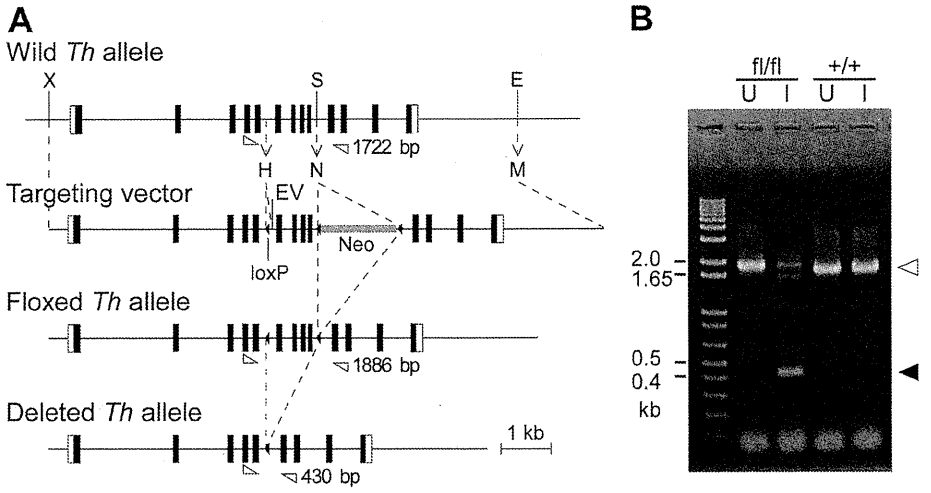

FIGURE 1. **Ablation of the *Th* gene by AAV-Cre injection into the SNc of the floxed *Th* mice.** *A*, schematic representation of the targeting vector for the generation of the floxed *Th* allele. *E*, EcoRI; *H*, HindIII; *M*, MluI; *N*, NotI; *S*, SpeI; *X*, XhoI; *Neo*, neomycin-resistant cassette. *Broken arrows* represent the generation or replacement of a restriction site. Exons are represented by *boxes*. The positions of the primers designed for the detection of genomic DNA recombination by PCR are indicated by *open triangles* with resulting PCR product sizes. *B*, PCR detection of genomic DNA recombination using primers for wild type (*open arrowhead*) or deleted *Th* (*closed arrowhead*) alleles. The template genomic DNA was prepared from the uninjected (*U*) or injected (*I*) side of the of the $Th^{fl/fl}$ or $Th^{+/+}$ mice 2 weeks after the unilateral microinjection of the AAV-Cre into the SNc. Note that the *Th* gene recombination was detected only in the injected side of the SNc of the $Th^{fl/fl}$ mice but not in the uninjected side of the $Th^{fl/fl}$ mice and the $Th^{+/+}$ mice.

$NaPO_4$ (pH 6.9) and a fluorescence detector (excitation 350 nm/emission 440 nm; RF-10A, Shimadzu, Tokyo).

Estimation of in Vivo L-DOPA Synthesis Activity per TH Protein Level—In vivo L-DOPA synthesis activity was evaluated by measuring the L-DOPA levels that accumulated in 30 min after the administration of 3-hydroxybenzylhydrazine dihydrochloride (NSD-1015, Sigma-Aldrich), an AADC inhibitor, to mice (100 mg/kg, intraperitoneal). The striatal tissues were homogenized using a pellet mixer (TreffLab) in 150 μl of PBS containing 1 mM dithiothreitol, 2 mM EDTA, 2 mM NaF, 1 μg/ml leupeptin, 1 μg/ml pepstatin, 1 mM phenylmethylsulfonyl fluoride, and 0.1 mM pargyline, followed by centrifugation at 20,000 × *g* for 10 min at 4 °C. An aliquot of the supernatant was used for assaying protein concentration by Bradford method, and Western blot to assess the TH protein levels. Another aliquot was deproteinized by 60 mM perchloric acid with 30 μM EDTA and 30 μM pargyline on ice for 30 min and centrifuged at 20,000 × *g* for 15 min. The supernatant was neutralized by K_2CO_3, and L-DOPA was purified by Al_2O_3 powder. The L-DOPA level was analyzed by HPLC with a NUCLEOSIL 100-7C18 reverse-phase column with a mobile phase buffer containing 0.1 M $NaPO_4$ (pH 3.5), 8 μM EDTA and electrochemical detection. To evaluate the *in vivo* L-DOPA synthesis activity per TH protein, L-DOPA accumulation was normalized to TH protein levels estimated by Western blot.

Rotation Test—Mice were placed in a round bowl (25 cm in diameter) for 20 min for acclimation. The mice were administered with 1-[2-[bis-(4-fluorophenyl)methoxy]ethyl]-4-(3-phenylpropyl)piperazine dihydrochloride (GBR12909; Tocris Bioscience; intraperitoneal, 30 mg/kg) and returned to the same bowl, and the behavior was videorecorded. The rotations were counted by visual observation for a 60-min period immediately after intraperitoneal injection. One rotation was defined by the animal completing a 360° turning without turning back in the opposite direction.

Statistics—The Mann-Whitney *U* test, Wilcoxon's signed rank test, or Steel's test was used as required. Spearman's rank correlation was used to evaluate a correlation between two groups. *p* values of <0.05 were considered significant. The data are shown as individual data points and mean values or as mean ± S.E., as indicated. Exponential and liner fittings were performed with Igor Pro 6.2 (WaveMetrics).

RESULTS

Production of Floxed Th Mice and Th Gene Ablation by AAV-Cre—First, we generated the floxed *Th* mice ($Th^{fl/fl}$) in which exons 6–9 of the *Th* gene were flanked by *loxP* sites (Fig. 1*A*). We used AAV-Cre to induce DNA recombination *in vivo* by performing a unilateral stereotaxic microinjection of the virus into the SNc of the adult floxed *Th* mice. Microinjection of AAV-Cre into the SNc induced DNA recombination in 2 weeks when we examined the substantia nigra tissue samples by PCR (Fig. 1*B*). *Th* gene recombination was detected in the injected side SNc of the $Th^{fl/fl}$ mice but not in the uninjected side of the $Th^{fl/fl}$ mice and both sides of the $Th^{+/+}$ mice. Thus, the floxed *Th* mice and AAV-Cre enabled us to induce *Th* gene ablation in the adult mouse midbrain.

Abrogation of TH Protein Expression in SNc Dopaminergic Neurons—Using immunohistochemistry, we next examined the effect of the AAV-Cre injection on TH protein expression in the SNc. The TH protein immunoreactivity was absent in the majority of neurons in the SNc 2 weeks after the AAV-Cre injection (Fig. 2*A* and *B*). We found that the number of TH-positive dopaminergic neurons normalized to the uninjected side was reduced by as early as 2 weeks, with the mean ratios of 38, 30, and 40% at 2, 4, and 8 weeks after the AAV-Cre injection, respectively, whereas they were unchanged in the $Th^{+/+}$ mice (97% at 8 weeks; Steel's test, $p = 0.0239$, 0.0166, and 0.0061 for the $Th^{fl/fl}$ mice at 2, 4, and 8 weeks, respectively, compared with the $Th^{+/+}$ at 8 weeks; Fig. 2*C*).

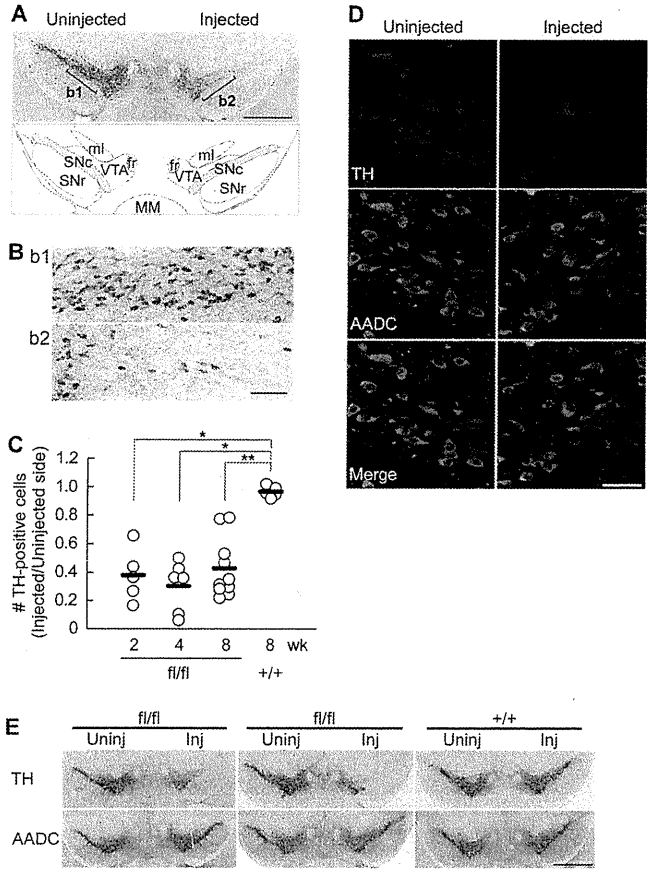

FIGURE 2. **AAV-Cre-induced loss of TH expression in the SNc.** *A*, a representative image of a midbrain slice immunostained for TH (*top*) and a schematic atlas (*bottom*). Serial coronal sections of the midbrains of the $Th^{fl/fl}$ mice were prepared 8 weeks after the AAV-Cre injection and were immunostained for TH. The SNc in the atlas is indicated by the *hatched area*. *fr*, fasciculus retroflexus; *ml*, medial lemniscus; *MM*, medial mammillary nucleus; *SNr*, substantia nigra pars reticulata; *VTA*, ventral tegmental area. *B*, magnified views of the uninjected side (*b1*) and injected side (*b2*) SNc as indicated in *A*. *C*, summary of the ratio of TH-positive cell numbers in the injected side SNc to the uninjected side. *Open circles* indicate the values from individual animals, and *bars* indicate the means. $n = 5$, 6, 11, and 5 brains for 2, 4, and 8 weeks ($Th^{fl/fl}$ mice) and 8 weeks ($Th^{+/+}$ mice) after injection, respectively. *, $p < 0.05$; **, $p < 0.01$, Steel's test. *D*, immunofluorescence staining for TH (*red*) and AADC (*green*) of the SNc of the $Th^{fl/fl}$ mice examined 2 weeks after the injection of AAV-GFP/Cre. TH and AADC were visualized with Alexa546 and Alexa633, respectively, distinguishing from GFP signal, and *pseudocolored* confocal images are shown. Note that the number of TH-expressing neurons was clearly reduced in the AAV-GFP/Cre-injected side, whereas the AADC, another dopaminergic neuron marker, remained expressed. *E*, TH deletion induces no apparent cell death in 16 weeks. Midbrain slices from two $Th^{fl/fl}$ mice and one $Th^{+/+}$ mouse were immunostained for TH and AADC 16 weeks after the AAV-Cre microinjection. Whereas the TH-expressing neurons were reduced in the injected side of the SNc of the $Th^{fl/fl}$ mice, the number of AADC-expressing neurons was apparently unaffected, suggesting that the dopaminergic neurons do not show cell death in the absence of TH in 16 weeks. *Scale bars*, 1 mm (*A*), 100 μm (*B*), 50 μm (*D*), and 1 mm (*E*).

To confirm a selective loss of TH protein, we also performed double immunofluorescence histochemistry for TH and aromatic AADC, a dopaminergic neuron marker. We used AAV-GFP/Cre for the purpose of labeling infected cells, but GFP expression in these neurons was too weak for detection, so we immunostained TH and AADC with Alexa546 and Alexa633 fluorophores, respectively, distinguishing from GFP signals. We found that the AADC immunoreactivity was preserved in the TH-negative neurons in the SNc 2 weeks after the AAV-GFP/Cre injection (Fig. 2*D*), suggesting that the AAV-GFP/Cre injection induced an efficient *Th* gene ablation without inducing cell death or damage. Moreover, AADC expression in the SNc was apparently unaffected in the $Th^{fl/fl}$ mice up to 16 weeks following the AAV-Cre injection, when the majority of the SNc dopaminergic neurons lost TH expression (Fig. 2*E*). These data suggest that dopamine is not essential for the survival of dopaminergic neurons in adult brains.

Slower Reduction of TH Proteins in Axon Terminals of Nigrostriatal Projection—The dopaminergic neurons in the SNc project their axons toward the striatum and form dense synapses (23, 24), where abundant TH proteins were contained. We quantitatively examined the reduction of the TH protein in the striatum by Western blot (Fig. 3*A* and *B*). The TH protein level was gradually reduced in the AAV-Cre injected side compared with the uninjected side in $Th^{fl/fl}$ mice, to 75, 50, and 39% at 2, 4, and 8 weeks after the AAV-Cre injection, respectively, whereas the levels were unchanged in the $Th^{+/+}$ mice (104% at 8 weeks; Steel's test, $p = 0.0932$, 0.0071, and 0.0059 for the $Th^{fl/fl}$ mice at 2, 4, and 8 weeks, respectively, compared with the $Th^{+/+}$ at 8 weeks; Fig. 3*B*). AADC protein levels did not show significant changes (Steel's test, $p = 0.77$, 0.92, and 0.88 for the $Th^{fl/fl}$ mice at 2, 4, and 8 weeks, respectively, compared with the $Th^{+/+}$ at 8 weeks; supplemental Fig. 2*A*).

We noticed that the reduction of TH protein level in the striatum could be slower than the reduction of the number of TH-expressing cells in the SNc because the difference between the two seemed remarkable at 2 weeks. To further investigate the difference, we compared the TH protein reductions in the striatum with that in ventral midbrain tissue, including SNc, using Western blot (Fig. 3*C*). We found that the TH protein reduction in the striatum showed a delay by about 2 weeks, whereas the decay time constants were similar ($\tau = 2.06$ and 2.04 weeks for the ventral midbrain and striatum, respectively).

We also used immunofluorescence histochemistry to examine the expression of TH and AADC in the striatum (Fig. 3*D*). Two weeks after the AAV-Cre injection, the number of TH-expressing axons in the injected side of the striatum of the $Th^{fl/fl}$ mice was only slightly reduced compared with the uninjected side, which was consistent with the Western blot data. However, the number of TH-expressing axons was decreased profoundly 8 weeks after the AAV-Cre injection. The number of AADC-expressing axons was apparently unchanged, suggesting that the axon terminals of the dopaminergic neurons remained mostly intact. These Western blot and immunohistochemical data indicate differential regulation of TH protein levels between axon terminals (striatum) and soma (SNc). Also, the *Th* gene ablation led to an almost complete and selective loss of TH protein in a subset of dopaminergic axons.

Better Maintenance of Striatal Dopamine Levels than TH Protein Levels—To investigate if dopamine levels follow the reduction of TH protein levels in the striatum, we assayed striatal monoamine contents using the same striatal extracts used in the Western blot analysis (Fig. 4*A*). The dopamine contents decreased gradually to around 98, 79, and 69% at 2, 4, and 8 weeks after the AAV-Cre injection, respectively, in the $Th^{fl/fl}$ mice but not in the $Th^{+/+}$ mice (104% at 8 weeks; Steel's test, $p = 0.98$, 0.0475, and 0.0637 for 2, 4, and 8 weeks in the $Th^{fl/fl}$

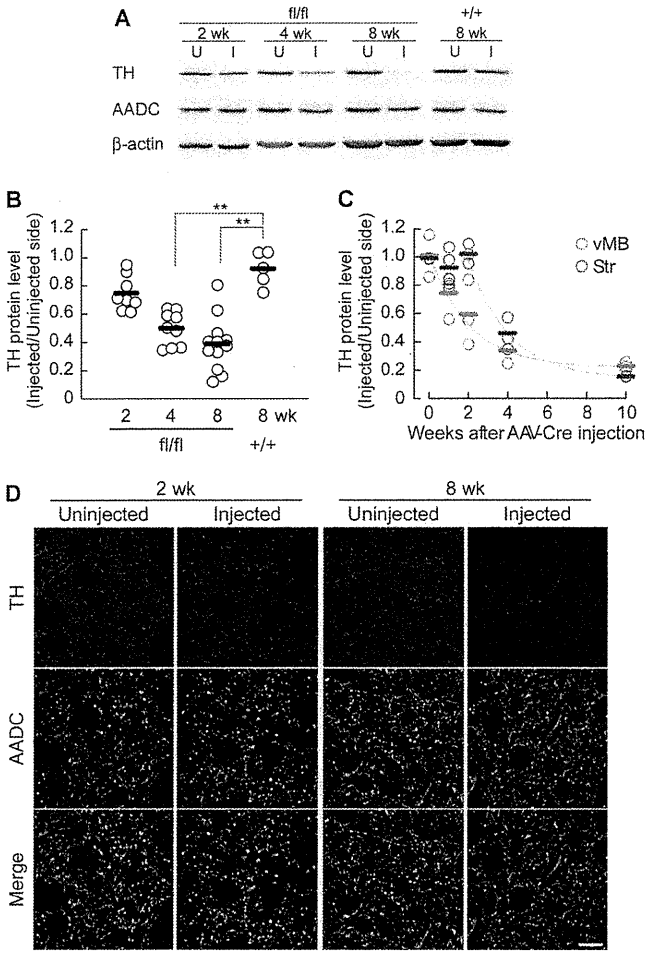

FIGURE 3. **Decrease in striatal TH protein levels after *Th* gene ablation.** *A*, striatal homogenates of each genotype were prepared 2, 4, or 8 weeks after the unilateral AAV-Cre injection into the SNc, and Western blot analysis was performed with antibodies against TH, AADC, and β-actin. *U* and *I*, uninjected and injected sides of the striatum, respectively. *B*, summarized quantitative analyses of Western blots for the striatal TH protein levels. The ratios of the protein level of the injected side to the uninjected side are plotted on the *vertical axis*. The *open circles* indicate the values from individual animals, and the *bars* indicate the means. $n = 8, 9, 12$, and 5 brains for 2, 4, and 8 weeks ($Th^{fl/fl}$ mice) and 8 weeks ($Th^{+/+}$ mice) after injection, respectively. *, $p < 0.05$; **, $p < 0.01$, Steel's test. *C*, comparison of TH protein levels in the striatum and ventral midbrain by Western blot. Tissue homogenates were prepared from the injected side and uninjected side of the ventral midbrain (*vMB*) and striatum (*Str*) of $Th^{fl/fl}$ mice and were subjected to Western blots for TH. $n = 2, 4, 3, 2$, and 3 for 0, 1, 2, 4, and 10 weeks after AAV-Cre injection, respectively. Data were fitted with an *exponential curve*. For the striatum, fitting was performed from 2 weeks because there was no apparent reduction before 2 weeks in this data set. *D*, decrease in the number of TH-expressing axons in the striatum. Striatal slices of the $Th^{fl/fl}$ mice were prepared 2 and 8 weeks after the injection of AAV-GFP/Cre and were immunohistochemically stained for TH (*red*) and AADC (*green*). TH and AADC were visualized as in Fig. 2*D*. *Merged images* are shown at the *bottom*. Images from the uninjected and injected side of the striatum are shown as indicated. *Scale bar*, 10 μm.

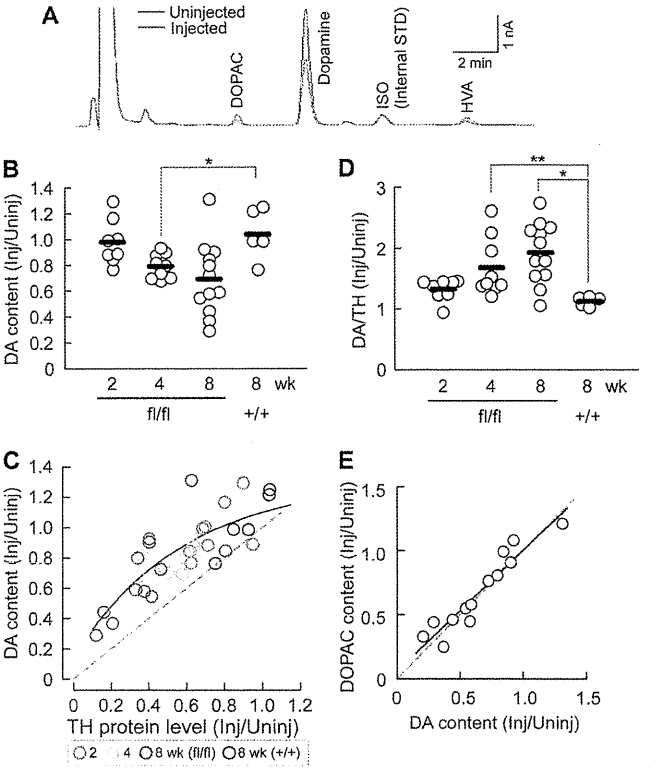

FIGURE 4. **The tissue dopamine contents are better maintained than TH protein levels in the striatum.** *A*, representative chromatograms of the monoamine assay with the homogenates from the uninjected and injected side striata from a $Th^{fl/fl}$ mouse 8 weeks after the injection of AAV-Cre. *B*, summarized DA contents in the striatum after the unilateral AAV-Cre injection to the SNc in the $Th^{fl/fl}$ and $Th^{+/+}$ mice. The monoamine assays were performed using the same extracts used in Fig. 3. The ratios of the dopamine contents in the injected side to the uninjected side are shown. The *open circles* indicate the values from individual animals, and the *bars* indicate the means. $n = 8, 9, 12$, and 5 brains for 2, 4, and 8 weeks ($Th^{fl/fl}$ mice) and 8 weeks ($Th^{+/+}$ mice) after the injection, respectively. *, $p < 0.05$, Steel's test. The mean dopamine contents in the uninjected side striata were 147.2 ± 10.2 and 158.1 ± 6.7 pmol/mg protein for $Th^{fl/fl}$ and $Th^{+/+}$ mice, respectively at 8 weeks (Steel's test, $p = 0.86$). *C*, the relationship between dopamine contents and TH protein levels. The *circles* represent data from individual animals and are *color-coded* by weeks after the AAV-Cre injection as indicated. The *dotted line* has a slope of 1. The *solid line* indicates an exponential curve fitting. The *points above* the *dotted line* suggest a higher dopamine level per TH protein level in the injected side compared with the uninjected side. *D*, ratio of the dopamine content to the TH protein level normalized to the uninjected side. $n = 8, 9, 12$, and 5 brains for 2, 4, and 8 weeks ($Th^{fl/fl}$ mice) and 8 weeks ($Th^{+/+}$ mice) after the injection, respectively. We excluded one outlier that showed very low TH protein levels and a high DA/TH ratio (29.8) from the 8-week $Th^{fl/fl}$ group. *, $p < 0.05$; **, $p < 0.01$, Steel's test. *E*, the relationship between DOPAC and dopamine contents in the $Th^{fl/fl}$ mice 8 weeks after the AAV-Cre injection. The data indicate the ratio of the DOPAC contents in the AAV-Cre-injected side of the striatum normalized to the uninjected side. The *open circles* indicate individual data. The *dotted line* has a slope of 1, and the *solid line* indicates a linear fitting. $n = 13$ mice. Spearman's rank correlation, $p < 0.0001$, $\rho = 0.96$ for DOPAC *versus* dopamine.

mice, respectively, compared with the $Th^{+/+}$ mice at 8 weeks; Fig. 4*B*). Notably, these reductions of dopamine contents were not as striking as those of TH protein levels (Fig. 2*C*). To evaluate the relationship between dopamine and TH, we plotted dopamine contents against TH protein levels (Fig. 4*C*). We found that dopamine contents were less affected than the TH protein levels, and the relationship was fitted well with an exponential curve ($\chi^2 = 0.7391$). The dopamine contents did not show a remarkable reduction until the TH protein levels were decreased by around 50%. Accordingly, the ratios of dopamine contents to TH protein levels were increased, with ratios of 1.32, 1.68, and 1.93 at 2, 4, and 8 weeks after the AAV-Cre injection, respectively, in the $Th^{fl/fl}$ mice, whereas it remained 1.1 in the $Th^{+/+}$ mice at 8 weeks (Steel's test, $p = 0.0665$, 0.0071, and 0.0157 for 2, 4, and 8 weeks for the $Th^{fl/fl}$ mice, respectively, compared with the $Th^{+/+}$ mice at 8 weeks; Fig. 4*D*).

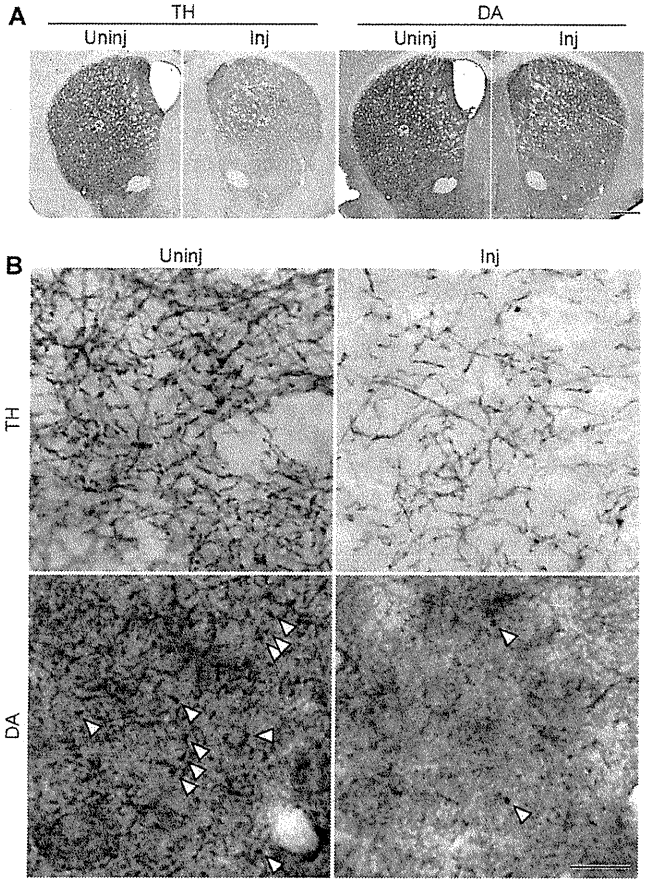

FIGURE 5. **TH and dopamine distribution in the striatum.** *A*, immunohistochemical detection of the striatal TH and DA in the striatum of the $Th^{fl/fl}$ mouse. The mice were fixed with glutaraldehyde 8 weeks after the injection of AAV-GFP/Cre, and the slices cut with a vibratome were stained with antibodies against TH or dopamine. Note that the TH signal in the injected side (*Inj*) was decreased compared with the uninjected side (*Uninj*), whereas the DA signal was less affected. *B*, magnification images of the regions indicated by *asterisks* in *A*, showing TH-expressing axon fibers and dopamine-containing axonal boutons. *Arrowheads* indicate representative puncta of the dopamine signals. *Scale bars*, 0.5 mm (*A*) and 10 μm (*B*).

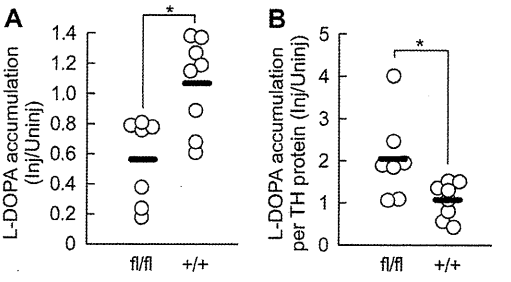

FIGURE 6. **Enhanced *in vivo* L-DOPA synthesis activity per TH protein level.** L-DOPA synthesis activities per TH protein level were estimated by measuring L-DOPA accumulation after *in vivo* administration of NSD-1015, an AADC inhibitor. Striatal homogenates were prepared 30 min after NSD-1015 administration (100 mg/kg, intraperitoneally). L-DOPA levels were measured by HPLC, and TH protein levels were assayed by Western blot. The mice were examined 8 weeks after the AAV-Cre injection. *A*, summary of L-DOPA accumulation in $Th^{fl/fl}$ and $Th^{+/+}$ mice. Data are shown as L-DOPA level in the injected side normalized by the uninjected side. The *open circles* indicate the values from individual animals, and the *bars* indicate the means. The mean L-DOPA level in the uninjected side of the $Th^{+/+}$ mice was 42.1 ± 7.3 pmol/mg protein. *B*, summary of L-DOPA accumulation normalized to the TH protein levels examined by Western blot, providing apparent L-DOPA synthesis activity per TH protein level. *, $p < 0.05$, Mann-Whitney *U* test.

It is known that unilateral depletion of dopamine in the rodent nigra induces ipsilateral rotation behavior in response to reagents enhancing dopaminergic transmission (25, 26). Consistently, $Th^{fl/fl}$ mice with severe unilateral dopamine depletion showed ipsilateral rotation behavior when administered with GBR12909, a potent DAT inhibitor (supplemental Fig. 2*B*), demonstrating the validity of our genetic manipulation to disrupt nigrostriatal dopaminergic transmission.

To further examine the tissue level alterations in the dopamine distribution, we used immunohistochemistry to determine the expression pattern for dopamine and TH in the striatum 8 weeks after the AAV-Cre injection. The mice were fixed transcardially with glutaraldehyde, and the striatal slices were stained with an antibody raised against dopamine-glutaraldehyde conjugate. We used immunoenzyme detection instead of immunofluorescence detection, because glutaraldehyde fixation causes a high fluorescence background. At a lower magnification, TH immunoreactivity was clearly reduced in the AAV-Cre-injected side of the $Th^{fl/fl}$ mice, whereas the dopamine immunoreactivity was only moderately reduced (Fig. 5*A*). These data are consistent with Western blot and monoamine assay results. Higher magnification views showed a reduction in the number of TH-expressing axon fibers in the AAV-Cre-injected side of the $Th^{fl/fl}$ mice (Fig. 5*B*) as observed by immunofluorescence staining (Fig. 3*D*). Moreover, the number of punctate signals of dopamine was also greatly decreased (Fig. 5*B*), suggesting that dopamine levels in the TH-lost axons were substantially reduced. Collectively, these data indicate a compensatory regulation of dopamine levels for a decrease in the TH protein levels. Because TH expression remained in only a subset of dopaminergic axons, these data raise the possibility that a decrease in dopamine synthesis induces a compensatory up-regulation of dopamine synthesis and/or storage in other axons.

Mechanisms of Dopamine Maintenance against TH Protein Loss—The homeostatic compensation of dopamine levels may accompany either an increase in the synthesis of dopamine or a decrease in the degradation of dopamine. To examine the degradation rate of dopamine, we measured the contents of 3,4-dihydroxyphenylacetic acid (DOPAC) and homovanillic acid (HVA), the two major metabolites of dopamine. Reductions of DOPAC and HVA contents were well correlated with that of dopamine in the $Th^{fl/fl}$ mice (Fig. 4*E*). Comparison between injected and uninjected sides showed no difference in the ratio of DOPAC to dopamine (DA) (injected side, 0.12 ± 0.02; uninjected side, 0.15 ± 0.03; Wilcoxon's signed rank test, $p = 0.16$) and in the ratio of HVA to dopamine (injected side, 0.13 ± 0.01; uninjected side, 0.14 ± 0.01; Wilcoxon's signed rank test, $p = 0.43$; supplemental Fig. 3). These data suggest that the degradation rate of dopamine was not significantly changed.

To explore a possible change in the activity of dopamine synthesis pathway, we evaluated *in vivo* L-DOPA synthesis activity by measuring L-DOPA accumulation 30 min after administration of NSD-1015, an AADC inhibitor, 8 weeks after the AAV-Cre injection. We found that the L-DOPA accumulation in the injected side of the striatum was significantly lower in the $Th^{fl/fl}$ mice compared with the $Th^{+/+}$ mice (Mann-Whitney *U* test, $p = 0.0206$; Fig. 6*A*). We then estimated the apparent L-DOPA

synthesis activity per TH protein by normalizing the L-DOPA accumulation with TH protein levels estimated by Western blot analysis. We found that the L-DOPA accumulation per TH protein in the injected side striatum was significantly higher in the $Th^{fl/fl}$ mice than in the $Th^{+/+}$ mice (Mann-Whitney *U* test, $p = 0.0279$; Fig. 6*B*). Considering that L-DOPA is mostly synthesized by TH (14), and the TH proteins remained to be expressed in only a subset of axons, these data suggest that dopamine synthesis activity in the remaining TH-positive axons was augmented to compensate for dopamine level.

Further, we examined if TH phosphorylation at Ser-31 and Ser-40 (27), the two major phosphorylation sites for TH activation, was elevated. However, we did not find a significant change in the phosphorylation states of these Ser residues by Western blot (supplemental Fig. 4). We also measured the contents of biopterin, an essential cofactor for TH, but the contents were not significantly different between the injected and uninjected side (uninjected side, 6.72 ± 0.54 pmol/mg protein; injected side, 6.64 ± 0.49 pmol/mg protein; Mann Whitney *U* test, $p = 0.95$). Thus, the long term up-regulation of L-DOPA synthesis activity may be supported by other molecular mechanisms (*e.g.* a relief of the feedback inhibition of TH by dopamine as a consequence of impaired dopamine synthesis).

In axon terminals, synthesized dopamine is primarily stored in synaptic vesicles, and released dopamine is partly recycled by DAT. When the number of TH-expressing axons was greatly reduced, the manner of dopamine storage could be changed for adaptation. In this context, we examined the level of two major dopamine transporters: vMAT2 and DAT. Western blot analysis showed no significant change in the vMAT2 and DAT protein levels in the injected side striatum compared with the uninjected side in the $Th^{fl/fl}$ mice, despite the great reduction of TH protein levels (supplemental Fig. 5). These data suggest that the numbers of dopaminergic synaptic vesicles and terminals were not grossly altered. Instead, because the majority of dopaminergic axons do not contain normal level of dopamine (Fig. 5*B*), despite the moderate decrease in tissue dopamine contents (Fig. 4), the vesicular dopamine contents in the TH-expressing axons may be increased, and/or TH-negative axons may uptake and contain low level dopamine.

DISCUSSION

Selective Loss of TH Protein in a Subset of Dopaminergic Neurons without Neuronal Degeneration—We took advantage of the Cre-*loxP* system in mice, which enabled us to selectively ablate the *Th* gene and block dopamine synthesis in adult brains. TH expression in the SNc was lost in a subset of SNc dopaminergic neurons by as early as 2 weeks after the AAV-Cre injection. The TH protein level and the number of TH-expressing axons in the striatum were clearly reduced 8 weeks after the AAV-Cre injection. Severe dopamine deficiency accompanied ipsilateral rotation behavior when stimulated with the DAT inhibitor, GBR12909, confirming the integrity of our genetic method to disrupt nigrostriatal dopaminergic transmission.

In contrast, the AADC protein levels and immunohistochemical signals in the striatum and SNc were unaffected 8 or 16 weeks after the AAV-Cre injection. These data suggest that the SNc dopaminergic neurons and axons were mostly preserved for several months without synthesizing dopamine. This is in contrast to neurodegenerative models using neurotoxins, such as 1-methyl-4-phenyl-1,2,3,6-tetrahydropyridine and 6-hydroxydopamine (6-OHDA), which could cause loss of axons and unpredictable side effects. Therefore, our experimental system provides a new animal model of chronic dopamine deficiency in adult brains without neuronal degeneration.

Differential Regulation of TH Protein Level in the Axon Terminals from Soma—Using this *Th* gene ablation strategy in adult brains, we noticed that the decline in the TH protein in the striatum was slower than the reduction of TH-expressing neurons in the SNc (Figs. 2*C* and 3*B*). By direct comparison of TH protein reduction in the striatum and ventral midbrain with Western blotting, we found that the TH protein reduction occurred in a delay, whereas the decay time constants were similar (Fig. 3*C*). This considerable delay of TH protein loss in the striatum suggests a mechanism that maintains the axonal TH protein level for a week or two without *Th* gene transcription. How does such a delay occur?

First, the turnover of TH proteins in axon terminals in the striatum may be slower than that in cell bodies in SNc. In cultured chromaffin cells, the steady-state half-life of the TH protein is about 1 day (28), but it could become longer than 10 days by treatment with translational inhibitors (29). Moreover, incubation with transcriptional inhibitors for 3 days caused no significant loss of the TH protein, although 90% of the TH mRNA was lost (29). Axonal translation may be involved for such a prolonged delay of protein degradation (30, 31). Thus, the difference in TH protein turnover in axon terminals and cell bodies located in SNc may be supported by those multiple regulatory mechanisms.

In addition, the delayed reduction of TH proteins may be attributable to slow axonal transport of TH proteins from soma to axons. Although the mechanism underlying axonal TH transport is not fully understood, the projection from SNc to the striatum in mice is about 2–10 mm, depending on axonal branching (22, 23). The axonal transport of TH was reported to be about 2 mm/h in chicken sciatic nerves (32), but it could be different in the brain because the cytosolic proteins are delivered by the slow axonal transport system at 0.1–8 mm/day (33, 34). These reports raise a possibility that it takes a week or more to transport TH proteins from a soma to axon terminals in the mouse nigrostriatal projection.

Regulation of Dopamine Levels by TH Protein Level and Activity in the Striatum—By quantitative comparison of dopamine contents with TH protein levels in the same striatal tissues, we found that dopamine contents were not simply determined by the TH protein level only. Notably, even 50% loss of TH protein did not remarkably change the dopamine contents. Eight weeks after the AAV-Cre injection, the TH protein levels were reduced to 39%, on average, whereas the dopamine contents were reduced to 69%. Immunohistochemical data showed a similar trend of difference. This finding is consistent with a previous report that dopamine contents in the brain of the adult $Th^{+/-}$ heterozygous mice are normally maintained despite a significant decrease in TH activity (12). Thus, these data indicate that the dopamine levels were primarily determined by TH

protein level but also influenced by another mechanism in the nigrostriatal projection.

In this study, we showed that (i) the TH protein expression was abrogated in a subset of dopaminergic neurons (AAV-Cre-infected neurons); (ii) the striatal dopamine contents were better maintained than the TH protein levels; and (iii) *in vivo* L-DOPA synthesis activity per TH protein level was enhanced. Because L-DOPA synthesis activity was virtually retained in only the TH-expressing axons, these results suggest that L-DOPA synthesis activity per TH protein in a given axon is partly affected by dopamine synthesis in the neighboring axons. Such trans-axonal regulation of dopamine synthesis activity might be a basis for the homeostasis of dopaminergic transmission in the striatum.

Consistent with our data, in a rat model of preclinical parkinsonism where nigrostriatal dopaminergic neurons were lesioned by 6-OHDA, TH activity was increased relative to dopamine loss (35). In such models generated with 6-OHDA, however, it is difficult to know if the enhanced TH activity observed after 6-OHDA administration is a result of a direct toxic effect of 6-OHDA on the remaining axons, a cell death of neighboring axons, or a decrease in tissue dopamine level. In contrast, our genetic manipulation specifically targets the *Th* gene in AAV-Cre-infected neurons, so our results demonstrate the effect of *Th* gene deletion on TH protein levels, dopamine contents, and L-DOPA synthesis activity more clearly and simply.

It remains to be determined how trans-axonal compensation of dopamine is mediated. For example, TH homospecific activity may be changed for the compensation by phosphorylation. D2 autoreceptors on dopaminergic axon terminals may be involved in controlling the dopamine level (36). However, it is not clear whether D2 autoreceptors modify dopamine synthesis in the long term. For example, chronic administration of haloperidol, a D2 receptor inhibitor, does not increase the basal levels of Ser(P)-31-TH and Ser(P)-40-TH in mice (37). We could not detect significant change in the Ser(P)-31-TH and Ser(P)-40-TH levels.

TH is also controlled by a feedback inhibition loop by dopamine (27). For example, a decrease in extracellular dopamine level by *Th* gene ablation may cause lower dopamine reuptake (38), lower local dopamine concentration in axon terminals, and a relief of TH from the feedback inhibition. Previous reports suggest that the concentration of released dopamine can be on the order of micromolar and is quickly taken up by DAT into dopaminergic axons (38). Because intracellular dopamine concentration is probably <100 nM (39), local intracellular dopamine concentration could be affected by dopamine reuptake. Meanwhile, TH has two dopamine-binding sites: high affinity (K_d < 4 nM) and low affinity (K_d = 90 nM) (40). Therefore, most TH proteins would be the dopamine-bound form for the high affinity site, whereas the low affinity site may be more relevant to feedback inhibition by dopamine (40).

Alternatively, there is a circuit level feedback (8) or neurotrophic factors, such as glial cell-derived neurotrophic factor (41). Further studies will be required to clarify the signaling mechanisms underlying the trans-axonal regulation of dopamine levels.

We found that the ratio of DOPAC and HVA contents to dopamine did not change, whereas, in Parkinson disease patients and model animals, DOPAC/DA and HVA/DA ratios were reported to be increased (7, 10, 42). This difference may exist because in our experimental conditions, most of the dopaminergic axons were preserved after the *Th* gene ablation, and those axons may have participated in the reuptake of extracellular dopamine, resulting in minimal effects on the dopamine degradation rate.

Adjusting Dopamine Storage for Compensation—If the number of dopamine-synthesizing axons was decreased by more than half, where and how were dopamine molecules stored for compensation? Because we did not observe any gross changes in the vMAT2 and DAT protein levels, it is unlikely that the numbers of dopaminergic synaptic vesicles and terminals were drastically changed. Otherwise, vesicular dopamine contents may be increased in the remaining TH-expressing axons for the compensation. For example, treatment of cultured dopaminergic neurons with L-DOPA or glial cell-derived neurotrophic factor increased vesicular dopamine levels more than 3-fold (41). Alternatively, it is also possible that the low level dopamine was contained in the TH-negative axons through the reuptake of spilled-over dopamine from neighboring synapses. This mechanism is consistent with the idea that released dopamine is spilled over and taken up by neighboring axons (38). Thus, the compensation of dopamine levels in our experimental system may accompany an increase in vesicular dopamine contents and/or spill-over and reuptake of released dopamine by TH-negative axons.

Taken together, in this study, we develop a conditional gene targeting method to efficiently and selectively inactivate the *Th* gene in the SNc dopaminergic neurons in adult mice without inducing neuronal degeneration. The analysis of these mutant mice revealed that TH protein levels in the axon terminals are regulated differently from the level in the soma, and the tissue dopamine levels are under trans-axonal compensatory regulation, where the reduction of dopamine in some axons induces up-regulation of dopamine synthesis activity in other axons. We believe that the present findings represent at least one of the compensatory mechanisms in Parkinson disease and are related to actions of remedies for psychiatric disorders.

Acknowledgments—We are most grateful to Professor Pierre Chambon for supporting this project. We thank Jean-Marc Bornert and the Institut de Génétique et de Biologie Moléculaire et Cellulaire/Institut Clinique de la Souris embryonic stem and mouse facility for excellent technical assistance. We thank Naomi Takino and Hiroko Nishida for technical assistance in constructing the AAV vectors. We thank Felix Schlegel for technical assistance with immunohistochemistry. We thank Dr. Pavel Osten for kindly providing the Synapsin I promoter construct.

REFERENCES

1. Graybiel, A. M., Canales, J. J., and Capper-Loup, C. (2000) *Trends Neurosci.* **23,** S71–S77
2. Schultz, W. (2007) *Trends Neurosci.* **30,** 203–210
3. Fahn, S. (2003) *Ann. N.Y. Acad. Sci.* **991,** 1–14
4. Grace, A. A., Floresco, S. B., Goto, Y., and Lodge, D. J. (2007) *Trends*

Neurosci. **30,** 220–227
5. Tye, K. M., Tye, L. D., Cone, J. J., Hekkelman, E. F., Janak, P. H., and Bonci, A. (2010) *Nat. Neurosci.* **13,** 475–481
6. Simpson, E. H., Kellendonk, C., Kandel, E. (2010) *Neuron* **65,** 585–596
7. Bernheimer, H., Birkmayer, W., Hornykiewicz, O., Jellinger, K., Seitelberger, F. (1973) *J. Neurol. Sci.* **20,** 415–455
8. Bezard, E., Gross, C. E., and Brotchie, J. M. (2003) *Trends Neurosci.* **26,** 215–221
9. McCallum, S. E., Parameswaran, N., Perez, X. A., Bao, S., McIntosh, J. M., Grady, S. R., and Quik, M. (2006) *J. Neurochem.* **96,** 960–972
10. Pifl, C., and Hornykiewicz, O. (2006) *Neurochem. Int.* **49,** 519–524
11. Perez, X. A., Parameswaran, N., Huang, L. Z., O'Leary, K. T., and Quik, M. (2008) *J. Neurochem.* **105,** 1861–1872
12. Kobayashi, K., Morita, S., Sawada, H., Mizuguchi, T., Yamada, K., Nagatsu, I., Hata, T., Watanabe, Y., Fujita, K., and Nagatsu, T. (1995) *J. Biol. Chem.* **270,** 27235–27243
13. Thomas, S. A., Matsumoto, A. M., and Palmiter, R. D. (1995) *Nature* **374,** 643–646
14. Zhou, Q. Y., Quaife, C. J., Palmiter, R. D. (1995) *Nature* **374,** 640–643
15. Zhou, Q. Y., and Palmiter, R. D. (1995) *Cell* **83,** 1197–1209
16. Szczypka, M. S., Kwok, K., Brot, M. D., Marck, B. T., Matsumoto, A. M., Donahue, B. A., and Palmiter, R. D. (2001) *Neuron* **30,** 819–828
17. Hnasko, T. S., Perez, F. A., Scouras, A. D., Stoll, E. A., Gale, S. D., Luquet, S., Phillips, P. E, Kremer, E. J., and Palmiter, R. D. (2006) *Proc. Natl. Acad. Sci. U.S.A.* **103,** 8858–8863
18. Nagatsu, T., Levitt, M., and Udenfriend, S. (1964) *J. Biol. Chem.* **239,** 2910–2917
19. Li, X. G., Okada, T., Kodera, M., Nara, Y., Takino, N., Muramatsu, C., Ikeguchi, K., Urano, F., Ichinose, H., Metzger, D., Chambon, P., Nakano, I., Ozawa, K., and Muramatsu, S. (2006) *Mol. Ther.* **13,** 160–166
20. Kadkhodaei, B., Ito, T., Joodmardi, E., Mattsson, B., Rouillard, C., Carta, M., Muramatsu, S., Sumi-Ichinose, C., Nomura, T., Metzger, D., Chambon, P., Lindqvist, E., Larsson, N. G., Olson, L., Björklund, A., Ichinose, H., and Perlmann, T. (2009) *J. Neurosci.* **16,** 15923–15932
21. Dittgen, T., Nimmerjahn, A., Komai, S., Licznerski, P., Waters, J., Margrie, T. W., Helmchen, F., Denk, W., Brecht, M., and Osten, P. (2004) *Proc. Natl. Acad. Sci. U.S.A.* **101,** 18206–18211
22. Paxinos, G., and Franklin, K. B. (2004) *The Mouse Brain in Stereotaxic Coordinates*, Academic Press, Inc., San Diego, CA
23. Prensa, L., and Parent, A. (2001) *J. Neurosci.* **21,** 7247–7260
24. Matsuda, W., Furuta, T., Nakamura, K. C., Hioki, H., Fujiyama, F., Arai, R., and Kaneko, T. (2009) *J. Neurosci.* **29,** 444–453
25. Ungerstedt, U., and Arbuthnott, G. W. (1970) *Brain Res.* **24,** 485–493
26. Lane, E. L., Cheetham, S., and Jenner, P. (2005) *J. Pharmacol. Exp. Ther.* **312,** 1124–1131
27. Dunkley, P. R., Bobrovskaya, L., Graham, M. E., von Nagy-Felsobuki, E. I., and Dickson, P. W. (2004) *J. Neurochem.* **91,** 1025–1043
28. Tank, A. W., Curella, P., and Ham, L. (1986) *Mol. Pharmacol.* **30,** 497–503
29. Fernández, E., and Craviso, G. L. (1999) *J. Neurochem.* **73,** 169–178
30. Lin, A. C., and Holt, C. E. (2008) *Curr. Opin. Neurobiol.* **18,** 60–68
31. Willis, D. E., and Twiss, J. L. (2006) *Curr. Opin. Neurobiol.* **16,** 111–118
32. Jarrott, B., and Geffen, L. B. (1972) *Proc. Natl. Acad. Sci. U.S.A.* **69,** 3440–3442
33. Terada, S. (2003) *Neurosci. Res.* **47,** 367–372
34. Hirokawa, N., Niwa, S., and Tanaka, Y. (2010) *Neuron* **68,** 610–638
35. Zigmond, M. J., Acheson, A. L., Stachowiak, M. K., and Stricker, E. M. (1984) *Arch. Neurol.* **41,** 856–861
36. Cubeddu, L. X., and Hoffmann, I. S. (1982) *J. Pharmacol. Exp. Ther.* **223,** 497–501
37. Håkansson, K., Pozzi, L., Usiello, A., Haycock, J., Borrelli, E., and Fisone, G. (2004) *Eur. J. Neurosci.* **20,** 1108–1112
38. Rice, M. E., and Cragg, S. J. (2008) *Brain Res. Rev.* **58,** 303–313
39. Mosharov, E. V., Larsen, K. E., Kanter, E., Phillips, K. A., Wilson, K., Schmitz, Y., Krantz, D. E., Kobayashi, K., Edwards, R. H., and Sulzer, D. (2009) *Neuron* **62,** 218–229
40. Gordon, S. L., Quinsey, N. S., Dunkley, P. R., and Dickson, P. W. (2008) *J. Neurochem.* **106,** 1614–1623
41. Pothos, E. N., Davila, V., and Sulzer, D. (1998) *J. Neurosci.* **18,** 4106–4118
42. Hefti, F., Enz, A., and Melamed, E. (1985) *Neuropharmacology* **24,** 19–23
43. Fukushima, T., and Nixon, J. C. (1980) Anal. Biochem. **102,** 176–188

Supplemental Figure Legends

Supplemental Fig. 1 Linearity in the quantification of TH proteins by Western blot.
Serial dilutions of striatal homogenates were prepared from the uninjected side of three mice and subjected to Western blot for TH. The linearity in the relationship between loaded protein level and detected TH signals was evaluated. Black, gray, and open circles represent data sets from individual mice. We employed a range showing linear relationship between actual loaded protein (2.5 to 20 μg, or 0.125 to 1.0 in ratios) and measured TH protein level (0.05 to 1 in ratio). The black line indicates a linear fitting. Dashed line has a slope of one.

Supplemental Fig. 2
A, Summarized quantitative analyses of Western blots for the striatal AADC protein levels. N = 8, 9, 13 and 5 brains for 2, 4, 8 weeks ($Th^{fl/fl}$ mice) and 8 weeks ($Th^{+/+}$ mice) after injection, respectively.
B, The relationship between rotation behavior and dopamine contents. 16 weeks after AAV-Cre injection, the mice were administered with DAT inhibitor, GBR12909 (30 mg/kg, i.p.), and ipsilateral rotation in 60 min was counted. One week later, striatal dopamine contents were measured. The dopamine content and ipsilateral rotation behavior showed significantly negative correlation (Spearman's rank correlation, $p = 0.0350$, $\rho = -0.94$). Gray line shows an exponential curve fitting.

Supplemental Fig.3 The relationship between dopamine and dopamine metabolites.
A, The relationship between HVA and dopamine contents in the $Th^{fl/fl}$ mice 8 weeks after the AAV-Cre injection. The data indicate the ratio of the HVA contents in the AAV-Cre injected side of the striatum normalized to the uninjected side. The open circles indicate individual data. The dotted line has a slope of one, and the solid line indicates a linear fitting. N = 13 mice. Spearman's rank correlation, $p = 0.0008$, $\rho = 0.97$ for HVA vs. dopamine.
B, Summarized ratios of the DOPAC and HVA to dopamine in the $Th^{fl/fl}$ mice 8 weeks after the AAV-Cre injection. (U) and (I) indicate the uninjected and injected sides of the striatum, respectively. Data indicate mean ± s.e.m..

Supplemental Fig. 4 Western blot analysis of the phospho-TH proteins.
A, pSer40-TH and pSer31-TH levels were examined by Western blot using antibodies against total, pSer40-, and pSer31-TH. Homogenates were prepared 8 weeks after the AAV-Cre injection.
B, *C*, Summary of scattered plots of pSer40-TH (*B*) and pSer31-TH (*C*) against total TH protein levels. Dotted lines have a slope of one. The protein levels of pSer40-TH and pSer31-TH are correlated to the total TH protein level in the $Th^{fl/fl}$ mice (Spearman's rank correlation, $p = 0.0054$, $\rho = 0.98$ for pSer40-TH vs. total TH; $p = 0.0063$, $\rho = 0.97$ for pSer31-TH vs. total TH). N = 6, 3 for $Th^{fl/fl}$ and $Th^{+/+}$, respectively. Note that there was no trend toward an increase in the ratio of phospho-TH to total TH protein level when total TH protein level was decreased.

Supplemental Fig. 5 Lack of changes in the striatal vMAT2 and DAT protein levels.
A, Representative Western blot for vMAT2 and DAT. Western blot was performed using crude synaptosomal fractions from the striatum of $Th^{fl/fl}$ mice prepared 8 weeks after AAV-Cre injection. The TH and β-actin protein levels were also examined. (U) and (I) indicate uninjected and injected side of the striatum, respectively. Note that while the TH protein level was reduced in the injected side, vMAT2 and DAT proteins did not show a reduction.
B, Summary of the quantification of Western blot data for vMAT2, DAT, and TH in the $Th^{fl/fl}$ and $Th^{+/+}$ mice. The ratios of protein levels in the injected side to the uninjected side are shown. The open circles indicate the values from individual animals, and the bars indicate the means. n

= 7, 3 for the $Th^{fl/fl}$ and $Th^{+/+}$, respectively. p = 0.31, 0.91, and 0.0167 for vMAT2, DAT, and TH, respectively, Mann-Whitney U test.

C, *D*, Relationship of protein levels between vMAT2 and TH proteins (*C*) or DAT and TH protein (*D*) were examined by scattered plots. The lines indicate linear fitting. There was no significant correlation (p = 0.42, 0.60 for vMAT2 vs. TH and DAT vs. TH, respectively, Spearman's rank correlation test).

Supplemental Fig. 1

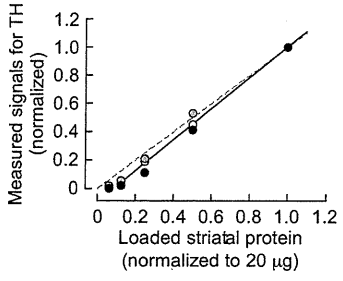

Supplemental Fig. 2

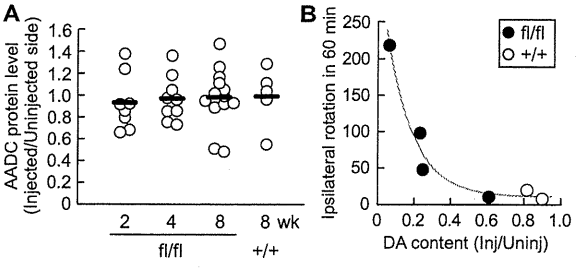

Supplemental Fig. 3

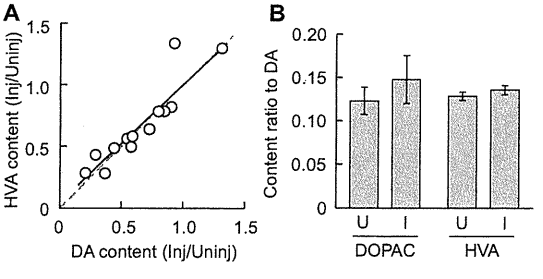

Supplemental Fig. 4

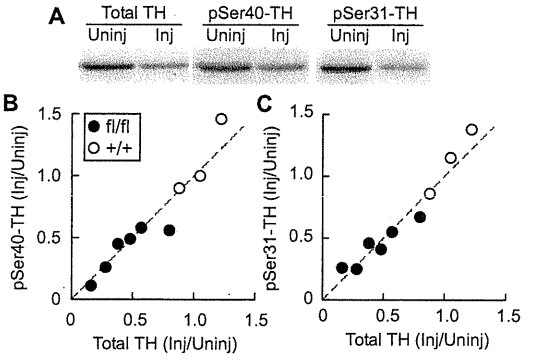

Supplemental Fig. 5

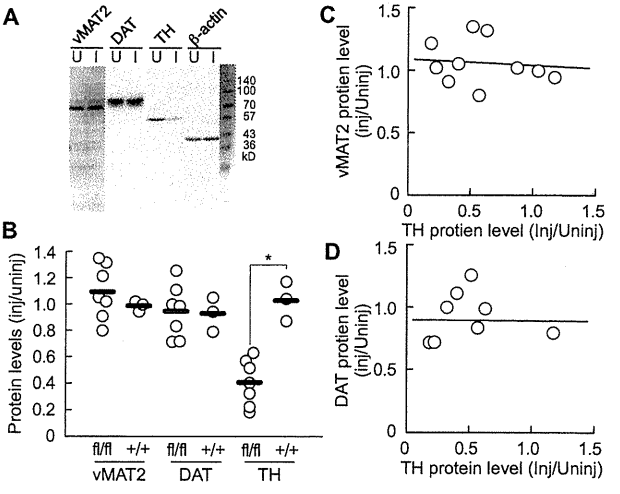

RESEARCH ARTICLE

Cortically Evoked Responses of Human Pallidal Neurons Recorded During Stereotactic Neurosurgery

Hiroki Nishibayashi, MD,[1]* Mitsuhiro Ogura, MD, PhD,[1] Koji Kakishita, MD, PhD,[1] Satoshi Tanaka, MD,[1] Yoshihisa Tachibana, DDS, PhD,[2] Atsushi Nambu, MD, PhD,[2] Hitoshi Kita, PhD,[3] and Toru Itakura, MD, PhD[1]

[1]*Department of Neurological Surgery, Wakayama Medical University, Wakayama, Japan*
[2]*Division of System Neurophysiology, National Institute for Physiological Sciences and Department of Physiological Sciences, The Graduate University for Advanced Studies, Okazaki, Japan*
[3]*Department of Anatomy and Neurobiology, College of Medicine, University of Tennessee Memphis, Memphis, USA*

ABSTRACT: Responses of neurons in the globus pallidus (GP) to cortical stimulation were recorded for the first time in humans. We performed microelectrode recordings of GP neurons in 10 Parkinson's disease (PD) patients and 1 cervical dystonia (CD) patient during surgeries to implant bilateral deep brain stimulation electrodes in the GP. To identify the motor territories in the external (GPe) and internal (GPi) segments of the GP, unitary responses evoked by stimulation of the primary motor cortex were observed by constructing peristimulus time histograms. Neurons in the motor territories of the GPe and GPi responded to cortical stimulation. Response patterns observed in the PD patients were combinations of an early excitation, an inhibition, and a late excitation. In addition, in the CD patient, a long-lasting inhibition was prominent, suggesting increased activity along the cortico-striato-GPe/GPi pathways. The firing rates of GPe and GPi neurons in the CD patient were lower than those in the PD patients. Many GPe and GPi neurons of the PD and CD patients showed burst or oscillatory burst activity. Effective cathodal contacts tended to be located close to the responding neurons. Such unitary responses induced by cortical stimulation may be of use to target motor territories of the GP for stereotactic functional neurosurgery. Future findings utilizing this method may give us new insights into understanding the pathophysiology of movement disorders. © 2011 *Movement* Disorder Society

Key Words: globus pallidus; microelectrode recording; cortical stimulation; stereotactic functional neurosurgery; Parkinson's disease; dystonia

Introduction

Deep brain stimulation (DBS) is a well-established treatment for advanced movement disorders, such as Parkinson's disease (PD).[1,2] Major targets of DBS are the globus pallidus (GP) and the subthalamic nucleus (STN). Although there is a trend toward targeting more at the STN, GP-DBS has several advantages, including amelioration of drug-induced dyskinesia and fewer adverse neuropsychological effects.[3] GP-DBS is also efficient to treat severe generalized or segmental dystonia.[4] The optimal target of GP-DBS is the posteroventral part of the internal segment of the GP (GPi), corresponding to its motor territory.[3,5–7] To identify the motor territory of the GPi, microelectrode recordings (MERs) of neuronal activity, such as spontaneous firing patterns and responses to passive and active movements, have been performed.[4,8,9]

Studies in nonhuman primates have shown that stimulation of the motor cortices can identify somatotopically organized motor territories in the external segment of the GP (GPe) and GPi.[10–13] In this study, we tested whether a similar method can be used to identify motor territories in the human GP. We recorded responses of GP neurons induced by motor cortical stimulation during stereotactic neurosurgery

Additional Supporting Information may be found in the online version of this article.

* **Correspondence to:** Hiroki Nishibayashi, Department of Neurological Surgery, Wakayama Medical University, 811-1 Kimiidera, Wakayama, 641-0012, Japan; hirokin@wakayama-med.ac.jp

Relevant conflict of interest/financial disclosures: Nothing to report. This study was supported by Wakayama Foundation for the Promotion of Medicine to T.I., Grants-in-Aid for Scientific Research (B) (18300135) from the Ministry of Education, Culture, Sports, Science and Technology of Japan and the Uehara Memorial Foundation to A.N., and NIH grants NS-47085 and NS-57236 to H. K.
Full financial disclosures and author roles may be found in the online version of this article.

Received: 26 April 2010; **Revised:** 1 September 2010; **Accepted:** 3 October 2010
Published online 10 February 2011 in Wiley Online Library (wileyonlinelibrary.com). DOI: 10.1002/mds.23502

of PD and cervical dystonia (CD) patients and compared them with responses of nonhuman primates. These data will also provide clues to understanding the pathophysiology of movement disorders.

Patients and Methods

Patients

This study was approved by the ethical committee of Wakayama Medical University and has followed its guidelines. The operations were performed on 10 PD patients and 1 CD patient (Supporting Information Table 1). The 8 male and 2 female PD patients were of mean age 61.9 years (range 50–72), had a mean disease duration of 126 months (48–168), and a mean levodopa dosage of 460 mg/day (300–800). Preoperative unified Parkinson's disease rating scale (UPDRS) was a mean best score of 25.3 (0–53) and a mean worst score of 66.6 (41–93). The 62-year-old female CD patient had a disease duration of 32 months and a Toronto western spasmodic torticollis rating scale (TWSTRS) score of 54. All patients received bilateral GP-DBS electrode implantation.

Surgical Procedure and MERs

Medications were withdrawn 18 hours before operation in most patients (Supporting Information Table 1). Surgery including MERs was performed without general anesthesia in most cases. Propofol was injected intravenously (2 mL/kg/hr) if necessary (patients 2, 5, and 11). Burr holes were made bilaterally on the coronal suture about 30 mm lateral from the midline. After dural incision, a strip electrode with four platinum discs (diameter of 5 mm) spaced 10 mm apart (UZN C1-04-04-10-1-A, Unique Medical; Tokyo, Japan) was inserted into the subdural space in the posterolateral direction and placed on the upper limb area of the primary motor cortex (MI). To avoid injury to the cortical veins, special care was taken during insertion of the strip electrode and no complications were noted. Electrical stimuli (1–20 mA strength, 1.0 ms duration monophasic constant current pulse at 1 Hz) were delivered through two of the four discs. A pair of discs inducing muscle twitches in the contralateral upper limb at the lowest intensity was selected and the motor threshold (T) was determined. In the following recordings, stimuli were delivered through this pair at the intensity inducing clear muscle twitches ($1.2–1.5 \times T$) at 1 Hz. A microelectrode (FC1002, Medtronic; Minneapolis, MN) was inserted through the same burr hole targeting the tentative target in the posteroventral GPi (20 mm lateral to the midline, 4 mm ventral to the intercommissural line, and 3 mm anterior to the midcommissural point), which was determined based on the magnetic resonance imaging (MRI). Neuronal activity was amplified, displayed (Leadpoint 9033A0315, Medtronic), and fed to a computer for on-line analysis. The responses induced by MI-stimulation were assessed by constructing peristimulus time histograms (PSTHs; bin width of 1 ms) for 20–120 stimulus trials using the software (LabVIEW 7.1, National Instruments; Austin, TX). Neuronal activity was also stored on a digital audio tape (DAT) recorder (PC204Ax, SONY; Tokyo, Japan) for off-line analysis. Somatosensory responses to joint manipulations and muscle palpations of the upper limb, lower limb, and orofacial regions were also examined. We performed only one or two recording electrode penetrations in each hemisphere because this was a trial study. The GPe/GPi border (the medial medullary lamina) and the ventral border of the GPi were identified by absence of unitary activity. Based on the MERs mappings, DBS electrodes (Model 3387, Medtronic) were implanted bilaterally into the same track of MERs. The deepest electrode contact was positioned within the GPi close to the ventral border. Pulse generators were later implanted bilaterally in the chest. Monopolar (the pulse generator was used as an anode) or bipolar stimulation was applied, and the most effective contacts of DBS electrodes to improve clinical symptoms were determined. Postoperative MRI verified the position of DBS electrodes in the posteroventral GPi, and the recording sites were estimated.

Off-line Data Analysis

Neuronal activity was played back from DAT, isolated by a window discriminator, converted into digital data, and fed to a computer. Responses induced by MI-stimulation were assessed by constructing PSTHs. The mean values and standard deviations of the firing rate during 100 ms preceding the stimulation onset were calculated from PSTHs and were considered to be the values for base discharge. Responses to MI-stimulation were judged to be significant if the firing rate during at least two consecutive bins (2 ms) reached the statistical level of $P < 0.05$ (one-tailed t-test). The latency of the response was defined as the time at which the firing rate first exceeded this level. Mean firing rates and patterns were analyzed from autocorrelograms (bin width, 0.5 ms) constructed from 50 s of digitized recordings. Spontaneous firing pattern was assessed by visual inspection of the autocorrelograms: Burst activity was inferred from the existence of a single peak, and oscillatory burst activity was inferred from multiple peaks and troughs.

Results

Neuronal activity was recorded at 163 sites along 27 electrode tracks in 21 hemispheres of 11 patients (Supporting Information Table 1). Single unit activity was isolated at 157 sites, and activity of 147 neurons (59 GPe and 88 GPi) was recorded long enough to

TABLE 1. Response patterns of GPe and GPi neurons evoked by cortical stimulation and numbers of oscillatory burst neurons recorded from the PD and CD patients

	GPe			GPi		
	Cortical stimulation			Cortical stimulation		
Patient	No. of responsive neurons/no. of neurons recorded	Response patterns and no. of neurons	No. of oscillatory burst neurons	No. of responsive neurons/no. of neurons recorded	Response patterns and no. of neurons	No. of oscillatory burst neurons
PD						
1	0/0		0	0/2		1
2	1/6	1 inh	2	2/6, (5/5)	2 inh, (1 inh+ex, 4 inh)	0, (2)
3	0/1		0	0/4		0
4	4/7	1 inh, 3 late ex	0	0/12		0
5	0/0, (0/2)		0	0/0		0
6	1/2	1 inh	1	1/4	1 ex+inh+ex	2
7	0/2		0	0/5		1
8	2/2	1 ex+inh+ex, 1 inh+ex	0	2/4	1 ex+inh, 1 late ex	3
9	4/10	4 inh	1	7/17	1 ex+inh, 1 inh+ex, 1 early ex, 1 inh, 3 late ex	0
10	6/15	1 ex+inh+ex, 3 inh+ex, 1 early ex, 1 inh	1	9/14	2 ex+inh+ex, 1 ex+inh, 2 inh+ex, 3 inh, 1 late ex	2
PD total	18/45, (0/2)	2 ex+inh+ex, 4 inh+ex, 1 early ex, 8 inh, 3 late ex	5	21/68, (5/5)	3 ex+inh+ex, 3 ex+inh, 3 inh+ex, 1 early ex, 6 inh, 5 late ex, (1 inh+ex, 4 inh)	9, (2)
CD						
11	4/11, (0/1)	1 ex+inh, 1 inh+ex, 1 inh, 1 late ex	6	6/13, (1/2)	2 ex+inh, 4 inh, (1 late ex)	1, (2)
Total	22/56, (0/3)		11	27/81, (6/7)		10, (4)

Numbers in parentheses, recorded under propofol
CD, cervical dystonia; ex, excitation; GPe and GPi external and internal segments of the globus pallidus; inh, inhibition; PD, Parkinson's disease.

construct PSTHs from at least 20 stimulus trials (mean of 43) (Table 1). Among them, 137 neurons (56 GPe and 81 GPi) were recorded without general anesthesia and used for further studies. The upper limb area of the MI was successfully identified in all hemispheres tested, and the stimulus intensity of 4–16 mA was used (Supporting Information Table 1).

Responses Evoked by MI-Stimulation

Among 137 neurons, MI-stimulation induced responses in 49 neurons (36%; 22/56 in GPe, 27/81 in GPi) (Table 1). In the PD patients, response patterns to MI-stimulation were combinations of an early excitation, an inhibition, and a late excitation (Fig. 1, A1–A4). A monophasic inhibition (Fig. 1, A1) was the major response pattern (36%; 8/18 in GPe, 6/21 in GPi). Other response patterns were also observed (Table 1): a biphasic response consisting of an inhibition and a subsequent excitation (Fig. 1, A2; 18%) or an excitation and a subsequent inhibition (8%); a triphasic response consisting of an early excitation, an inhibition and a late excitation (Fig. 1, A3 and A4; 13%); and a monophasic early (5%) or late (20%) excitation. On the other hand, in the CD patient, a long-lasting monophasic inhibition (Fig. 1, A5; 50%) and a long-lasting inhibition preceded by an excitation (Fig. 1, A6; 30%) were the typical response patterns (Table 1).

The latency and duration of each component are compared in Table 2. The durations of the inhibitions in the GPe and GPi of the CD patient were significantly longer than those of the PD patients, respectively (t-test, $P < 0.05$). The latency of the inhibition in the GPi of the CD patient was significantly longer than that of the PD patients (t-test, $P < 0.01$).

Spontaneous Activity

Among 137 neurons, spontaneous activity of 71 neurons (28 GPe and 43 GPi) was recorded long enough for analysis. The mean firing rates of GPe and GPi neurons in the PD patients were significantly higher than those of GPe and GPi neurons in the CD patient, respectively (Table 2; t-test, $P < 0.05$). Besides 71 neurons, activity of six neurons was recorded under propofol administration and had a tendency to decreased activity.

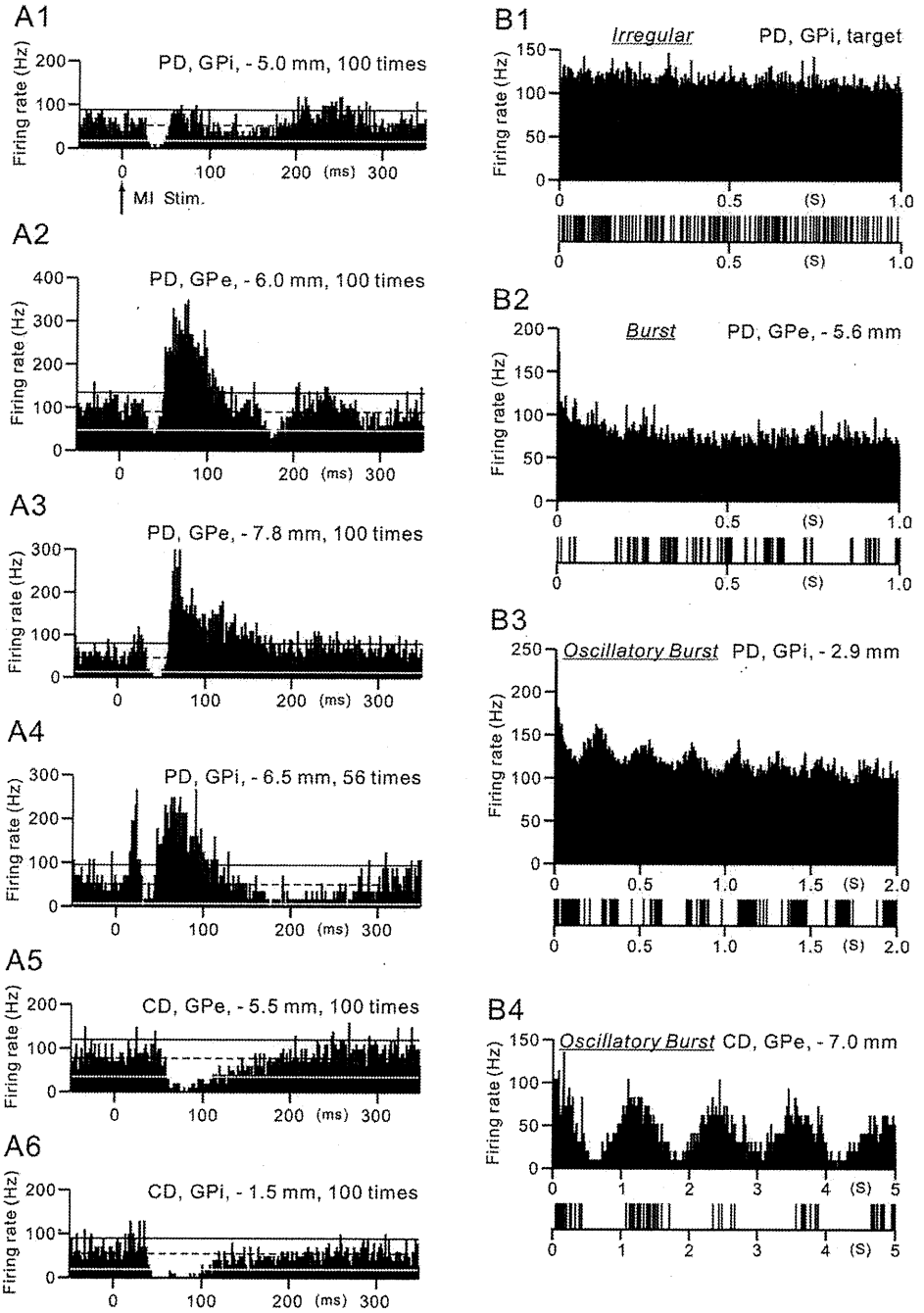

FIG. 1. A: Peristimulus time histograms (PSTHs; bin width of 1 ms) showing the responses of neurons in the external (GPe) and internal (GPi) segments of the globus pallidus evoked by stimulation of the upper limb area of the primary motor cortex in the Parkinson's disease (PD) (A1–A4) and cervical dystonia (CD) (A5 and A6) patients. Cortical stimulation was given at time = 0 (arrow in A1). Recorded sites indicated by the distance from the tentative target (negative distance, above the target) and the numbers of stimulus trials were also shown. The mean firing rate and the statistical levels of $P < 0.05$ (one-tailed *t*-test) calculated from the firing rate during 100 ms preceding the onset of stimulation are indicated by black dotted lines (mean), a black solid line (upper limit of $P < 0.05$), and a white solid line (lower limit of $P < 0.05$), respectively. **B**: Autocorrelograms and slow traces of digitized spikes of GPe and GPi neurons recorded from the PD (B1–B3) and CD (B4) patients. Neuronal activity can be classified into irregular, burst, and oscillatory burst types.

Based on the slow traces of digitized spikes and autocorrelograms, spontaneous firing patterns could be classified into three types: irregular, burst, and oscillatory burst (Fig. 1, B). Irregular neurons fired randomly and were characterized by the flat autocorrelogram (Fig. 1, B1). Burst neurons showed grouped discharges and a single peak around time 0 in the autocorrelogram (Fig. 1, B2). Oscillatory burst neurons showed repetitive grouped discharges and multiple cycles of peaks and troughs in the

TABLE 2. Latencies and durations of cortically evoked responses and spontaneous firing rates in GPe and GPi neurons of the PD and CD patients

	PD		CD	
	GPe	GPi	GPe	GPi
Latency (mean ± SD, ms)				
Early excitation	22.3 ± 5.0 (n = 3)	22.5 ± 8.8 (n = 7)	22.0 (n = 1)	22.0 ± 4.2 (n = 2)
Inhibition	32.6 ± 11.1(n = 14)	34.2 ± 9.9[a] (n = 15)	46.0 ± 4.6 (n = 3)	48.7 ± 7.9[a] (n = 6)
Late excitation	60.7 ± 14.4 (n = 9)	56.2 ± 14.3 (n = 11)	79.0 ± 31.1(n = 2)	(-)
Duration (mean ± SD, ms)				
Early excitation	6.3 ± 7.5 (n = 3)	5.8 ± 4.4 (n = 7)	16.0 (n = 1)	2.5 ± 0.71 (n = 2)
Inhibition	16.1 ± 7.4[b] (n = 14)	19.1 ± 12.2[c] (n = 15)	42.3 ± 34.6[b] (n = 3)	37.5 ± 15.6[c] (n = 6)
Late excitation	27.6 ± 33.7 (n = 9)	25.7 ± 39.2 (n = 11)	2.5 ± 0.71 (n = 2)	(-)
Spontaneous firing rate	81.0 ± 52.5[d] (n = 17)	92.7 ± 40.1[e] (n = 34)	45.8 ± 17.6[d] (n = 11)	62.3 ± 12.1[e] (n = 9)
(mean ± SD, Hz)	[-]	[47.2 ± 23.6 (n = 3)]	[46.7 (n = 1)]	[27.1 ± 36.7 (n = 2)]

Values in brackets, recorded under propofol.
[a] $P < 0.01$.
[b,c,d,e] $P < 0.05$, significantly different from each other (t-test).

autocorrelogram (Fig. 1, B3 and B4). Most neurons [94% (16/17) in GPe and 68% (23/34) in GPi in PD, 100% (11/11) in GPe and 78% (7/9) in GPi in CD] showed burst or oscillatory burst activity (Table 3). In the PD patients, more GPe neurons showed burst or oscillatory burst activity than GPi neurons ($P < 0.05$, Fisher's exact test). Oscillatory frequency of oscillatory burst neurons in the PD patients was mostly in the delta (1–4 Hz) or theta–alpha (4–12 Hz) band, while that in the CD patient was mostly in the delta band.

Locations of Recorded Neurons

Locations of recorded neurons are plotted in Figure 2. GPe/GPi neurons responding to MI-stimulation were found in clusters along electrode tracks, although the rostral and the lateral part of the GPe were not explored. Among 49 GPe/GPi neurons responding to MI-stimulation, 12 neurons (24%) responded to passive movements of the upper limb, such as shoulder, elbow, wrist, or digits. On the other hand, among 43 GPe/GPi neurons responding to passive movements of the upper limb, 12 neurons (28%) responded to MI-stimulation. Neurons responding to passive movements of the lower limb were found in the different area from the upper limb area. Neurons responding to jaw movements were mainly found in the ventral to middle part of the GPi.

Correlation between Clinical Benefits and Neuronal Responses

Monopolar (14 sides) or bipolar (eight sides) electrical stimulation (1.5–3.5 V constant voltage, 210 μs duration, at 185 Hz) was applied for DBS. The most effective cathodal contacts were located in the dorsal (11 sites), middle (two sites), ventral (six sites) GPi, or ventral GPe (three sites; Fig. 2, Supporting Information Table 2). For the PD patients, symptoms were assessed using UPDRS III and IV (items 18–35) before and 10–20 days after starting DBS (Supporting Information Table 2). Symptoms were ameliorated in all patients, and the DBS was markedly effective (score ≥ 10) in four patients (patients 2, 6, 8, and 10) and fairly effective (score ≥ 5) in other four patients (patients 3, 4, 7, and 9). Noticeably improved symptoms (score ≥ 4) were rigidity (patients 2, 3, 7, 8, and 10), bradykinesia (patients 2, 6, 8, and 10), tremor (patients 4, 6, and 8), and dyskinesia (patient 10). In the CD patient, the TWSTRS score decreased from 54 to 34, and unilateral cervical rotation was markedly improved. The most effective cathodal contacts tended to be located close to the responding neurons (Fig. 2).

Discussion

Responses Evoked by MI-Stimulation

In this study, the responses of GPe/GPi neurons induced by MI-stimulation were composed of various combinations of an early excitation, an inhibition, and a late excitation in human subjects. In the GPe, GPi and substantia nigra pars reticulata (SNr) of monkeys

TABLE 3. Spontaneous firing patterns of GPe and GPi neurons recorded from the PD and CD patients

	PD		CD	
Spontaneous firing pattern	GPe	GPi	GPe	GPi
Irregular	1	11	0	2
Burst	11	14	5	6
Oscillatory burst	5	9	6	1
<4 Hz	3	3	6	1
4–12 Hz	2	5	0	0
12 Hz<	0	1	0	0
Total	17	34	11	9

Numbers of GPe and GPi neurons exhibiting irregular, burst, or oscillatory burst activity are shown.

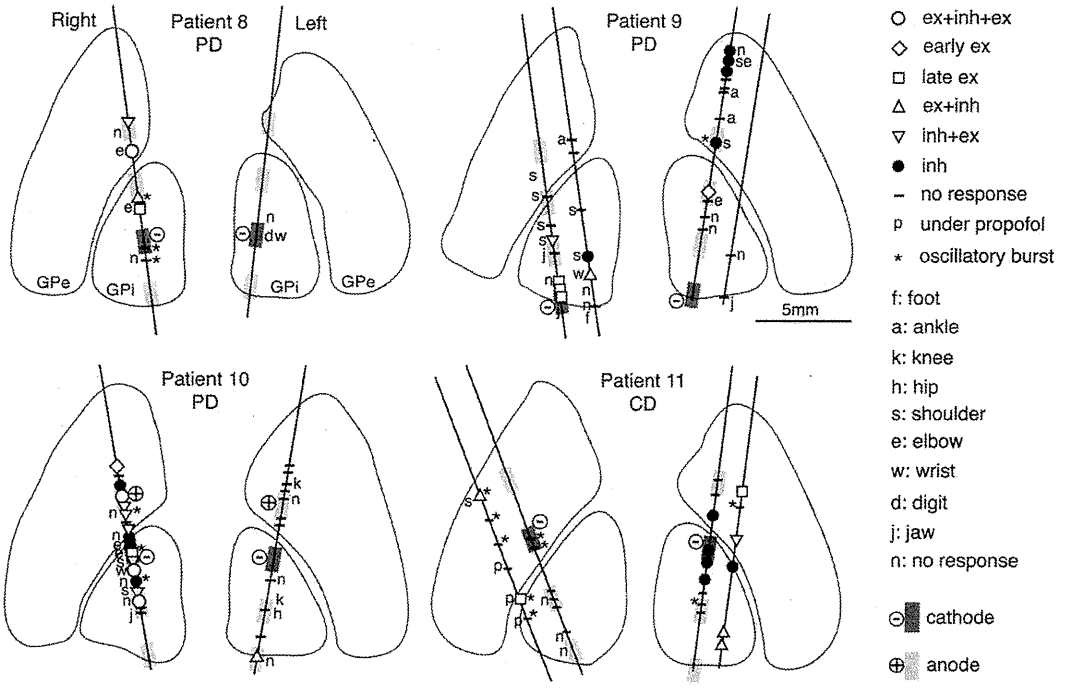

FIG. 2. Locations of recorded neurons in the GPe and GPi of the PD (patients 8, 9, and 10) and CD (patient 11) patients shown in coronal views. Response patterns evoked by cortical stimulation and somatosensory inputs examined by passive manipulations were represented by different symbols. Locations of DBS electrodes were also shown by shaded rectangles (dark rectangle with minus sign, the most effective cathode; light rectangle with plus sign, anode used). In patients 8, 9, and 11, monopolar stimulation was performed using the pulse generator as an anode.

and rodents, cortical stimulation evoked typically a triphasic response, composed of an early excitation, an inhibition, and a late excitation,[10–16] which is very similar to the triphasic response observed in this study (Fig. 1, A3 and A4). Studies in nonhuman primates have clarified that the early excitation is derived from the cortico-STN-GPe/GPi pathway,[10] the inhibition by the cortico-striato-GPe/GPi pathway, and the late excitation by the cortico-striato-GPe-STN-GPe/GPi pathway.[12,13] We assume that the response components observed in the present human study were derived from the same pathways. However, a major response pattern in human patients was a monophasic inhibition. Such a pattern difference may be ascribed to the stimulus methods. Although stimulating wire electrodes were implanted inside the cortex of animals, disc electrodes on the cortical surface in this study may less effectively stimulate cortico-STN neurons, which are located in the deeper layer than corticostriatal neurons. The latencies of response components in this study (Table 2) were two times longer than those in monkeys[10–13] and three times longer than those in rodents.[14–16] These latency differences may be ascribed to the following reasons: (1) larger size of the human brain; (2) surface electrodes in this study may stimulate cortical neurons indirectly through afferent fibers or apical dendrites, whereas wire electrodes in animal studies may stimulate directly and instantly somata and axons; (3) pathological changes in PD.

Somatotopic Representations in the GPe/GPi

The somatotopic representations in the GPe/GPi have been repeatedly studied by movement-related activity during task performance, somatosensory inputs from muscles and joints, responses evoked by cortical stimulation and anatomical methods in nonhuman primates.[11,17,18] In the caudal part of the GPe/GPi, the orofacial area is represented in the most ventral part, and the lower limb area is found in the dorsal part. The upper limb area is located in between. The similar somatotopic representations were also reported in humans during stereotactic surgery.[19] The upper limb area occupies a large region in the GPe/GPi and is a good target to search during surgery. In this study, we have succeeded in identifying the upper limb area in the GPe/GPi by neuronal responses evoked by MI-stimulation, as well as by somatosensory inputs.

Targeting the Motor Territories of the GPe/GPi

The motor territory of the GPi is usually identified during stereotactic surgery by conventional electrophysiological methods, such as observing responses to passive/active movements.[8,9] The method introduced in this study, examining the unitary responses induced by MI-stimulation, can also identify the motor territories of the GPe/GPi. Some neurons that responded to MI-stimulation did not show somatosensory responses

probably because stimulus conditions were not optimal, especially during surgery. The effective cathodal contacts tended to be located close to the responding neurons. On the other hand, this method is more complex and time-consuming than the conventional ones, and thus, it is more appropriate in special cases, such as in patients under sedation, with considerable damage or with previous lesions in the basal ganglia; when spontaneous firing patterns or somatosensory responses are less obvious; and in cases aimed for research purposes.

Pathophysiology of Movement Disorders

There are many reports on GPe/GPi activity in PD patients and parkinsonian monkeys.[20–23] Decreased activity along the striato-GPi direct pathway and increased activity along the striato-GPe indirect pathway have been considered to cause increased GPi activity and finally interfere with disinhibitory process of releasing appropriate movements in PD.[24] Although not significant, firing rate of GPi neurons was higher than that of GPe neurons in this study (Table 2), supporting the firing rate theory. However, this study failed to show difference in durations of inhibitions between GPe and GPi neurons. Contrary to the firing rate theory, recent studies have focused on abnormal burst and oscillatory activity in the GPe/GPi underlying the PD pathophysiology.[25] Most neurons in this study showed burst or oscillatory burst activity.

On the other hand, reports on GPe/GPi activity in CD patients are limited.[26] The GPi firing rate in CD patients was lower than that in PD patients. GPi neurons fired in a more irregular pattern with more frequent and longer pauses in CD patients compared with PD patients. GPe/GPi activity in generalized dystonia decreased and became bursty.[27,28] The present data showed decreased GPe/GPi activity in the CD patient compared with the PD patients, and burst and oscillatory burst activity, agreeing with the previous reports.[26] Moreover, MI-stimulation induced a long-lasting inhibition in the GPe/GPi (Fig. 1, A5 and A6), suggesting increased activity along the cortico-striato-GPe/GPi pathway. Recently, the mouse model of dystonia also showed a long-lasting inhibition evoked by cortical stimulation in the GPe/GPi,[16] which is very similar to that observed in this study. Thus, increased activity along both the cortico-striato-GPi direct and cortico-striato-GPe indirect pathways is considered to be a fundamental change in dystonia. Reduced GPi output should disinhibit thalamic and cortical activity, resulting in involuntary movements observed in dystonia.

References

1. Rodriguez-Oroz MC, Obeso JA, Lang AE, et al. Bilateral deep brain stimulation in Parkinson's disease: a multicentre study with 4 years follow-up. Brain 2005;128:2240–2249.
2. Volkmann J, Allert N, Voges J, Sturm V, Schnitzler A, Freund HJ. Long-term results of bilateral pallidal stimulation in Parkinson's disease. Ann Neurol 2004;55:871–875.
3. Peppe A, Pierantozzi M, Altibrandi MG, et al. Bilateral GPi DBS is useful to reduce abnormal involuntary movements in advanced Parkinson's disease patients, but its action is related to modality and site of stimulation. Eur J Neurol 2001;8:579–586.
4. Starr PA, Turner RS, Rau G, et al. Microelectrode-guided implantation of deep brain stimulators into the globus pallidus internus for dystonia: techniques, electrode locations, and outcomes. J Neurosurg 2006;104:488–501.
5. Lombardi WJ, Gross RE, Trepanier LL, Lang AE, Lozano AM, Saint-Cyr JA. Relationship of lesion location to cognitive outcome following microelectrode-guided pallidotomy for Parkinson's disease: support for the existence of cognitive circuits in the human pallidum. Brain 2000;123:746–758.
6. Vitek JL, Bakay RA, Hashimoto T, et al. Microelectrode-guided pallidotomy: technical approach and its application in medically intractable Parkinson's disease. J Neurosurg 1998;88:1027–1043.
7. Yelnik J, Damier P, Bejjani BP, et al. Functional mapping of the human globus pallidus: contrasting effect of stimulation in the internal and external pallidum in Parkinson's disease. Neuroscience 2000;101:77–87.
8. Hutchison WD, Lozano AM.Microelectrode recordings in movement disorder surgery. In: Lozano AM, editor. Movement disorder surgery. Basel: Karger; 2000. p 103–117. (Progress in Neurological Surgery; Vol. 15).
9. Kaplitt MG, Hutchison WD, Lozano AM.Target localization in movement disorders surgery. In: Tarsy D, Vitek JL, Lozano AM, editors. Surgical treatment of Parkinson's disease and other movement disorders. Totowa: Humana Press; 2003. p 87–98.
10. Nambu A, Tokuno H, Hamada I, et al. Excitatory cortical inputs to pallidal neurons via the subthalamic nucleus in the monkey. J Neurophysiol 2000;84:289–300.
11. Yoshida S, Nambu A, Jinnai K. The distribution of the globus pallidus neurons with input from various cortical areas in the monkeys. Brain Res 1993;611:170–174.
12. Kita H, Nambu A, Kaneda K, Tachibana Y, Takada M. Role of ionotropic glutamatergic and GABAergic inputs on the firing activity of neurons in the external pallidum in awake monkeys. J Neurophysiol 2004;92:3069–3084.
13. Tachibana Y, Kita H, Chiken S, Takada M, Nambu A. Motor cortical control of internal pallidal activity through glutamatergic and GABAergic inputs in awake monkeys. Eur J Neurosci 2008; 27:238–253.
14. Maurice N, Deniau JM, Glowinski J, Thierry AM. Relationships between the prefrontal cortex and the basal ganglia in the rat: physiology of the cortico-nigral circuits. J Neurosci 1999;19: 4674–4681.
15. Ryan LJ, Clark KB. The role of the subthalamic nucleus in the response of globus pallidus neurons to stimulation of the prelimbic and agranular frontal cortices in rats. Exp Brain Res 1991;86: 641–651.
16. Chiken S, Shashidharan P, Nambu A. Cortically evoked long-lasting inhibition of pallidal neurons in a transgenic mouse model of dystonia. J Neurosci 2008;28:13967–13977.
17. DeLong MR, Crutcher MD, Georgopoulos AP. Primate globus pallidus and subthalamic nucleus: functional organization. J Neurophysiol 1985;53:530–543.
18. Strick PL, Dum RP, Picard N. Macro-organization of the circuits connecting the basal ganglia with the cortical motor areas. In: Houck JC, Davis JL, Beiser DG, editors. Models of information processing in the basal ganglia. Cambridge: MIT Press; 1995. p 117–130.
19. Guridi J, Gorospe A, Ramos E, Linazasoro G, Rodriguez MC, Obeso JA. Stereotactic targeting of the globus pallidus internus in Parkinson's disease: imaging versus electrophysiological mapping. Neurosurgery 1999;45:278–287; discussion 287–279.
20. Bergman H, Wichmann T, Karmon B, DeLong MR. The primate subthalamic nucleus. II. Neuronal activity in the MPTP model of parkinsonism. J Neurophysiol 1994;72:507–520.
21. Raz A, Vaadia E, Bergman H. Firing patterns and correlations of spontaneous discharge of pallidal neurons in the normal and the tremulous 1-methyl-4-phenyl-1,2,3,6-tetrahydropyridine vervet model of parkinsonism. J Neurosci 2000;20:8559–8571.

22. Hutchison WD, Levy R, Dostrovsky JO, Lozano AM, Lang AE. Effects of apomorphine on globus pallidus neurons in parkinsonian patients. Ann Neurol 1997;42:767–775.

23. Magnin M, Morel A, Jeanmonod D. Single-unit analysis of the pallidum, thalamus and subthalamic nucleus in parkinsonian patients. Neuroscience 2000;96:549–564.

24. DeLong MR. Primate models of movement disorders of basal ganglia origin. Trends Neurosci 1990;13:281–285.

25. Brown P. Abnormal oscillatory synchronisation in the motor system leads to impaired movement. Curr Opin Neurobiol 2007;17:656–664.

26. Tang JK, Moro E, Mahant N, et al. Neuronal firing rates and patterns in the globus pallidus internus of patients with cervical dystonia differ from those with Parkinson's disease. J Neurophysiol 2007;98:720–729.

27. Vitek JL, Chockkan V, Zhang JY, et al. Neuronal activity in the basal ganglia in patients with generalized dystonia and hemiballismus. Ann Neurol 1999;46:22–35.

28. Starr PA, Rau GM, Davis V, et al. Spontaneous pallidal neuronal activity in human dystonia: comparison with Parkinson's disease and normal macaque. J Neurophysiol 2005;93:3165–3176.

EUROPEAN JOURNAL OF NEUROSCIENCE

European Journal of Neuroscience, Vol. 34, pp. 1470–1484, 2011 doi:10.1111/j.1460-9568.2011.07865.x

NEUROSYSTEMS

Subthalamo-pallidal interactions underlying parkinsonian neuronal oscillations in the primate basal ganglia

Yoshihisa Tachibana,[1,2] Hirokazu Iwamuro,[1] Hitoshi Kita,[3] Masahiko Takada[4] and Atsushi Nambu[1,2]
[1]Division of System Neurophysiology, National Institute for Physiological Sciences, Okazaki, Aichi, Japan
[2]Department of Physiological Sciences, The Graduate University for Advanced Studies, Okazaki, Aichi, Japan
[3]Department of Anatomy and Neurobiology, College of Medicine, University of Tennessee Health Science Center, Memphis, TN, USA
[4]Systems Neuroscience Section, Primate Research Institute, Kyoto University, Inuyama, Aichi, Japan

Keywords: GABA, globus pallidus, glutamate, parkinsonian monkeys, subthalamic nucleus

Abstract

Parkinson's disease is characterized by degeneration of nigral dopaminergic neurons, leading to a wide variety of psychomotor dysfunctions. Accumulated evidence suggests that abnormally synchronized oscillations in the basal ganglia contribute to the expression of parkinsonian motor symptoms. However, the mechanism that generates abnormal oscillations in a dopamine-depleted state remains poorly understood. We addressed this question by examining basal ganglia neuronal activity in two 1-methyl-4-phenyl-1,2,3,6-tetrahydropyridine-treated parkinsonian monkeys. We found that systemic administration of L-3,4-dihydroxyphenylalanine (L-DOPA; dopamine precursor) decreased abnormal neuronal oscillations (8–15 Hz) in the internal segment of the globus pallidus (GPi) and the subthalamic nucleus (STN) during the ON state when parkinsonian signs were alleviated and during L-DOPA-induced dyskinesia. GPi oscillations and parkinsonian signs were suppressed by silencing of the STN with infusion of muscimol ($GABA_A$ receptor agonist). Intrapallidal microinjection of a mixture of 3-(2-carboxypiperazin-4-yl)-propyl-1-phosphonic acid (CPP; *N*-methyl-D-aspartate receptor antagonist) and 1,2,3,4-tetrahydro-6-nitro-2,3-dioxo-benzo[*f*]quinoxaline-7-sulfonamide (NBQX; AMPA/kainate receptor antagonist) also decreased the oscillations in the GPi and the external segment of the globus pallidus (GPe). Neuronal oscillations in the STN were suppressed after intrasubthalamic microinjection of CPP/NBQX to block glutamatergic afferents of the STN. The STN oscillations were further reduced by muscimol inactivation of the GPe to block GABAergic inputs from the GPe. These results suggest that, in the dopamine-depleted state, glutamatergic inputs to the STN and reciprocal GPe–STN interconnections are both important for the generation and amplification of the oscillatory activity of STN neurons, which is subsequently transmitted to the GPi, thus contributing to the symptomatic expression of Parkinson's disease.

Introduction

Degeneration of nigral dopaminergic neurons is associated with motor symptoms of Parkinson's disease (PD), which include bradykinesia, rigidity, and tremor. Changes in the firing rates of basal ganglia (BG) neurons are thought to induce the PD symptoms (Albin *et al.*, 1989; DeLong, 1990). Contrary to the rate-based theory, the pathophysiology of PD is often correlated with abnormal burst firing and oscillatory activity in the BG (Filion, 1979; Wichmann *et al.*, 1994; for reviews, see Boraud *et al.*, 2002; Brown, 2003; Gatev *et al.*, 2006; Rivlin-Etzion *et al.*, 2006a; Hammond *et al.*, 2007). Single/multi-unit activity and local field potentials (LFPs) recorded from parkinsonian animals and patients have shown that oscillatory activity and neuronal synchronization in the globus pallidus and the subthalamic nucleus (STN) include two major frequency bands: the 'tremor-related' 3–8-Hz band and the higher 8–30-Hz band (Bergman *et al.*, 1994; Levy *et al.*, 2000; Brown *et al.*, 2001). However, the mechanisms regulating the abnormal BG oscillations remain unknown.

The first goal of the present study was to examine whether parkinsonian BG oscillations might depend on dopaminergic inputs. Dopamine therapy can ameliorate parkinsonian signs and, at least partly, reverse the abnormal firing pattern of spike trains (Boraud *et al.*, 1998; Levy *et al.*, 2001a, 2002; Heimer *et al.*, 2006; Lafreniere-Roula *et al.*, 2010) and neuronal synchronization observed in LFPs (Brown *et al.*, 2001; Cassidy *et al.*, 2002; Priori *et al.*, 2004) in the BG. However, little is known about systemic dopamine-dependent changes in the firing properties of neurons of the internal segment of the globus pallidus (GPi), external segment of the globus pallidus (GPe) and STN in the same parkinsonian subject. Thus, we tested the effects of intravenous L-3,4-dihydroxyphenylalanine (L-DOPA) injection on BG neuronal activity in 1-methyl-4-phenyl-1,2,3,6-tetrahydropyridine (MPTP)-treated monkeys (Fig. 1A). The second

Correspondence: Atsushi Nambu and Yoshihisa Tachibana, [1]Division of System Neurophysiology, as above.
E-mails: nambu@nips.ac.jp and banao@nips.ac.jp

Received 20 May 2011, revised 3 August 2011, accepted 8 August 2011